



Journal of Applied and Computational Mechanics



Research Paper

Numerical and Experimental Investigation on Post-buckling Behavior of Stiffened Cylindrical Shells with Cutout subject to Uniform Axial Compression

Amir Reza Shahani¹, Faraz Kiarasi^{1,2}

¹ Department of Applied Mechanics, Faculty of Mechanical Engineering, K.N. Toosi University of Technology, 19395-1999, Tehran, Iran, Emails: shahani@kntu.ac.ir; faraz_kia@email.kntu.ac.ir

² Department of Mechanical engineering, University of Eyvanekey, Eyvanekey, Semnan, Iran

Received May 18 2020; Revised March 15 2021; Accepted for publication March 15 2021.

Corresponding author: A.R. Shahani (shahani@kntu.ac.ir)

© 2021 Published by Shahid Chamran University of Ahvaz

Abstract. In this paper, post buckling behavior of thin steel and aluminum cylindrical shells with rectangular cutouts under axial loading was studied experimentally and also using the finite element method. Riks method is used for analyzing the cylindrical shells. The effect of longitudinal and circumferential stiffeners (ribs and stringer) was studied on the buckling load and the post buckling behavior as the stiffeners used individually and in combination with each other. It was shown that by adding stringer, the buckling load improves and the rib has a positive effect on the post buckling behavior of the structure. Some tests were performed by ZwickRoell tensile/compression testing machine and it was carried out for both types of steel and aluminum shells with and without stiffeners. Comparing the experimental results with the FEA results shows good agreement. Nonlinear analysis of cylindrical steel and aluminum shells with cutout have demonstrated that, in some cases, a local buckling called snap-back can be seen in the load-displacement path. Snap-back which is a decrease in the amount of both load and displacement indicates this local buckling. This phenomenon is because of appearing mode shapes sequentially during the numerical buckling analysis of shells. Although these local buckling happened, the structure is still endured the higher loads.

Keywords: Post-buckling, Stiffened Shells, Rib, Stringer, cutout, buckling test.

1. Introduction

Buckling is a hazardous phenomenon which causes sudden failure of the structure and as a result leads to life or economic losses. Therefore, it is significant to study the buckling behavior if one engages the design of slender structures under compressive load, which exists commonly in large steel structures of mining, marine, offshore and construction industries. The load region that a structure enters after buckling is called post-buckling area. Generally, before final failure occurs, there may be considerable load capacity beyond buckling. This is true particularly for plates, in contrast to beams, may have significant load-carrying ability beyond buckling. The first initiation of buckling is often related to mode shapes obtained from a modal frequency analysis Eslami [1]. Cylindrical shells are widely used in aerospace and automotive industries and some submarine structures [2]. Their performance is to transmit the axial loading, and thus to be under pressure.

Aircraft fuselages contain several cutouts of different shapes. Most common of which are the rectangular openings. Cutouts are required either for access or for the passage of piping, uptakes, ventilation ducts and electrical systems in cylindrical shells. Buckling load of these shells are adversely affected by the cutout size, owing to causing local stiffness variations that lead to stress concentrations and also local buckling. Furthermore, considering the small thickness of walls, the occurrence of imperfections is possible, which reduce the amount of critical buckling stress additionally. The imperfections in thin cylinders are grouped as geometrical and material imperfections. For increasing the capacity of these structures, it is necessary to strengthen them. Cylindrical shells with stiffeners have suitable characteristics against different loads. It means stringers and ribs reinforce shells to provide high load-carrying capacities. Many structural investigators all over the world study the buckling and post buckling of cylindrical shells made by different materials. The stress distribution around an opening in the cylindrical shells with cutout under axial, internal and torsional compressive loadings are computed by Van Dyke [3]. Tennyson [4] studied the effects of circular cutout of cylindrical shells under axial compression. Almroth and Brogan [5] investigated the influence of the rectangular cutouts on the elastic axial buckling strength with the STAGS computer codes. They also studied the cylindrical shell with two circular cutouts, both numerically and experimentally [6]. Toda [7] investigated the cylindrical shells with circular cutouts under axial compression and studied the effect of stiffness around the cutouts as well Hilburger et al., [8] has assessed the buckling of composite cylindrical shells with square cutouts under combined internal pressure and axial compression. Results denoted that out of plane displacement near the cutout only can be affected by internal pressure load and size of cutout. Estekhnachi and Vafai [9] have studied



the buckling behavior of isotropic cracked cylindrical shells subjected to axial loading by using the classical finite element method. Frulloni et al. [10] studied instability of reinforced hollow structures under external hydrostatic loading for aerospace applications using finite element and experimental methods. Rahimi and Poursaeedi [11] investigated the plastic analysis of cylindrical shells with a single circle cutout subjected to bending moment using the analytical method. Ghorbanpour Arani et al. [12] have investigated elastic stability of rib and stringer-stiffened cylindrical shells subjected to axial compression and internal and external pressures. The stiffeners are ribs, stringers and their different designs at the inner and outer of the shell. Finally, using the Ritz method to obtain critical buckling loads. Han et al. [13] has used nonlinear numerical method in ANSYS software to investigate the effects of size and location of square cutouts on the thin- and thick-walled cylindrical shells and provided several parametric relations based on their analytical and empirical results. Buermann et al. [14] contemplated an analysis for local post-buckling analysis of stringer and frame-stiffened cylindrical panels. They studied the influence of local skin buckling and stiffener tripping. For the stiffeners, a uniaxial membrane stress state is supposed while plane stress state is considered for the skin. Shariati and Rokhi [15] studied FEM analysis of thin steel cylindrical shells with different lengths and diameters with elliptical cutouts. They developed many parametric relationships for both the numerical and experimental results using the Lagrangian polynomial method Shariati and Rokhi [16]. Also, Shariati and Rokhi [17] investigated a similar numerical study by using ABAQUS software to perform the response of steel cylindrical shells with the elliptical cutout under bending moment and also the effect of various lengths and diameters of shell and cutout are analyzed. They performed some relations for computing buckling moment of these structures. Bisagni and Cordisco [18] studied buckling of cylindrical shell with internal stringers and external rings under mixed axial compression and torsion experimentally. Yazdani and Rahimi [19] investigated buckling load of cylindrical shell with two kinds of internal stiffeners, i.e. lozenge and triangular. The buckling of steel cylindrical shell reinforced by rib and stringer is investigated by Shahani and Mohammadjani [20]. Finally, the results obtained from ABAQUS software have been compared with analytical relations. Furthermore, an effort has been done to extract the finite element instability load vs structure reinforcement. Cheng et al. [21] investigated the geometrical imperfection effects on the buckling behavior of thin-walled cylindrical shells under compression by both experimental and numerical methods. The imperfections were created by one or two circular cutouts on the shell surface. A three-dimensional (3D) Digital Image Correlation Method was used for experimental investigation. Jiao et al. [22] studied the ring stiffener effects on the buckling behavior of cylindrical shells with cutout subjected to axial compression by both experimental and numerical investigation. They used the finite element method to simulate the displacement controlled compression tests. Brunesi and Nascimbene [23] considered the effects of cutouts on the buckling strength of cylindrical shells. They studied the buckling and post-buckling response of a large set of cylindrical steel thin-shell with structural openings. Liang et al. [24] performed Nonlinear buckling analysis of the conical and cylindrical shells using the simplified Green-Lagrange (SGL) and strain based on reduced order method and the polynomial homotopic continuation (PHC) method the PHC method. They used the polynomial homotopic continuation (PHC) method. In addition, Vu-Bac et al. [25] presented a NURBS-based Inverse analysis for reconstruction of nonlinear deformations of Thin Shells. They derived FE equations of thin shells and using gradient-based algorithms in this method. Also, various instabilities were taken into account like snap-through and snap-back.

The above literature review shows that many studies have been conducted about the buckling analyses of unstiffened shells with and without cutout, and also the effects of shape, size and location of cutouts on buckling load are investigated in several researches. It was concluded that for all cutout shapes, critical buckling load decreases when cutout area is decreased. Also, by remaining the cutout area constant and changing the shape of cutouts, it was observed that the buckling load did not change noticeably. However, rounded shapes are less critical. Thus, the cut out area is the most significant parameter on the critical buckling load. Thus, the experimental and numerical post buckling analysis of cylindrical shell reinforced by both rib and stringer with cutout can be helpful to clarify and develop post-buckling issues because there are many difficulties in the process of analyzing a cylindrical shell with cutout.

Many similar researches have been conducted. However, to the best of author's knowledge, some previous papers have shown local buckling, like snap back, in their numerical analysis but they did not study the occurrence of this phenomenon experimental. In previous works discussed about snap back, they did not provide any experimental analysis to compare the results, like Ref [28]. While in this work, the numerical and experimental postbuckling paths of stiffened cylindrical shells are compared, and we showed when this local buckling occurred in numerical curve, how the experimental post buckling curve will be. Another novel point of this paper is the use of both stringer and rib as stiffeners in cylindrical shells with riveted joints. In other words, the riveted joints have been modelled in accordance with the real physics of the fabricated shells. Moreover, specimen dimensions of the previous experimental investigations presented in the literature review were more or less small rather than the shells fabricated for conducting the tests of the present study, and even the big ones, like Ref. [22], are unstiffened. We also consider various imperfection amplitudes by writing codes in the Abaqus software, to find the most proper amplitudes for getting the best agreement between numerical and experimental results. While, previous works did this just for unstiffened shells. In this work, comparison between numerical and experimental of cylindrical shells which have unstable behavior in their numerical post-buckling path, like snap-back, are provided. Nonlinear analyses using the ABAQUS finite element software, which is based on first order shear deformation theory, were accomplished to find the effect of cutouts and stiffeners on the buckling and post-buckling behavior of cylindrical shells. Nonlinear analysis of cylindrical steel and aluminum shells with cutout have shown, in some cases, before the global buckling occurs, a local buckling can be seen in the load-displacement path. Snap-back, which is a decrease in the amount of both load and displacement, indicates this local buckling. Although these local buckling happened, the structure is still tolerated higher loads. In other cases, global instability occurs immediately after reaching the critical load. The shell collapse after buckling, so it cannot tolerate higher loads and the load decreases gradually. The local buckling called Snap-back cannot be seen in experimental results but during the numerical buckling analysis of shells, mode shapes appear sequentially, commonly called mode jumps or mode transitions. Therefore, the local buckling which is obtained by the Riks method is important for predicting behaviors in designing structures.

Moreover, it will be shown that the influence of using stringer in increasing buckling load is stronger than rib-stiffened one. Also, by using rib as a stiffener, the shell will endure higher loads in post-buckling path. Six thin-walled cylindrical shells were fabricated for conducting some tests, three of them were made from steel and the other three from aluminum. Each set contains an unstiffened cylinder and two similar stiffened cylinders (for repeating the test to increase accuracy). Both rib and stringer are used in these stiffened specimens.

2. Experimental procedure

The schematic configuration of the cylindrical shell with cutout in some engineering applications is shown in Fig. 1.

2.1. Materials and geometry of test specimens

Six thin-walled cylindrical shells were fabricated for conducting some tests, three of them were made from steel and the other



three from aluminum. Each set contains an unstiffened cylinder and two similar stiffened cylinders (repeating the test to increase accuracy). Both rib and stringer are used in these stiffened specimens, 2 ribs are outside and 4 stringers are inside the cylinder. The length, diameter and thickness of cylindrical shells are 400 mm, 250 mm and 1.5 mm, respectively. Also, the geometry of rib and stringers is as shown in Fig 2. The thickness of stiffeners is 1.5 mm. All specimens have 2 cutouts symmetrically at the middle of shell length. Length and width of the rectangular cutout are 70 and 40 mm, respectively.

The stiffened cylindrical shells used for this study were made of mild steel alloy and aluminum alloy. The mechanical properties of this steel alloy and aluminum were determined according to ASTM E8 standard [26].

Based on the linear portion of stress-strain curve, which is shown in Figs 3, the value of elasticity modulus for steel alloy and aluminum alloy are presented in Table 1. Stress-strain behavior of Material C and D exhibit power-law model. At least eight points can be defined to estimate the actual behavior of this plastic model.

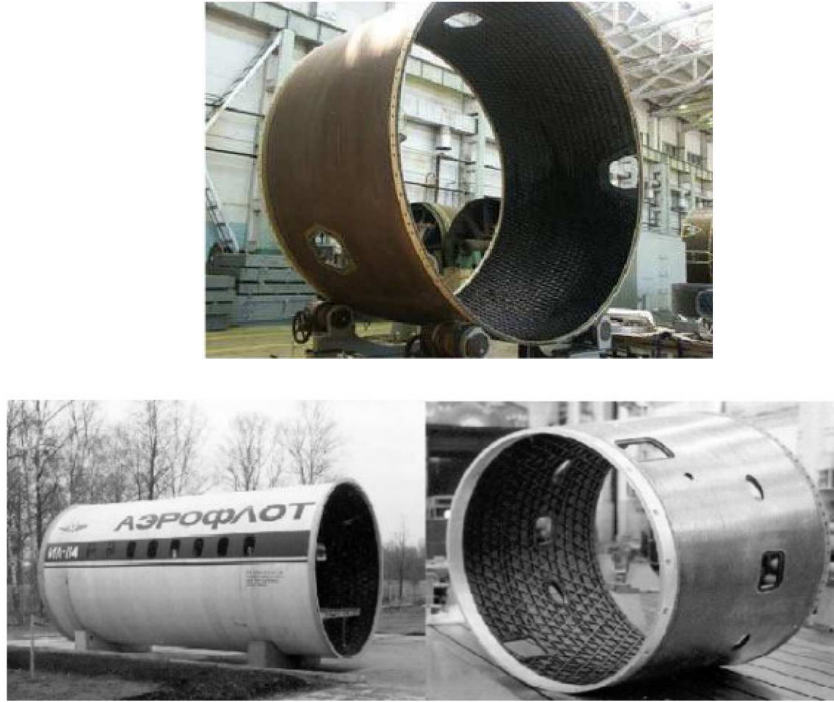


Fig. 1. The schematic configuration of the cylindrical shell with cutout

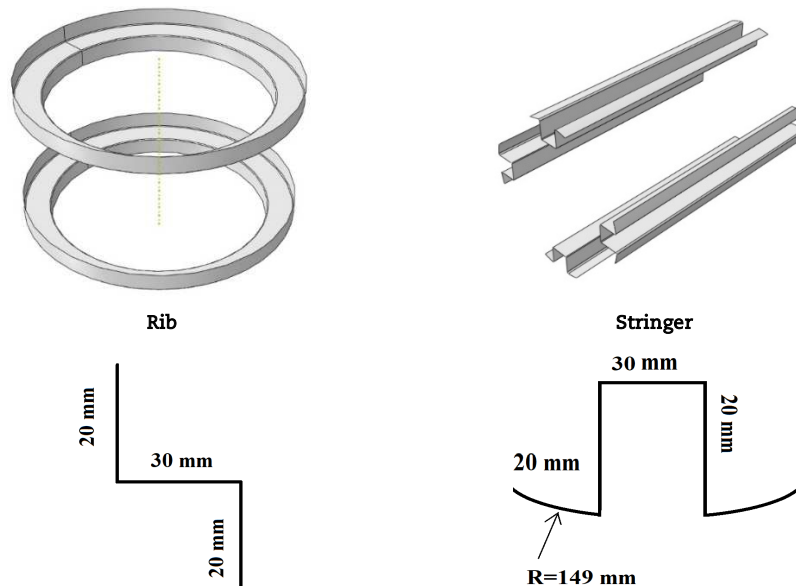


Fig. 2. Geometry of ribs and stringers

Table 1. Mechanical properties of specimens

Type	Material	Elasticity modulus E (GPa)	Poisson's ratio ν
C	Steel	195.6	0.285
D	Aluminum	71.856	0.326



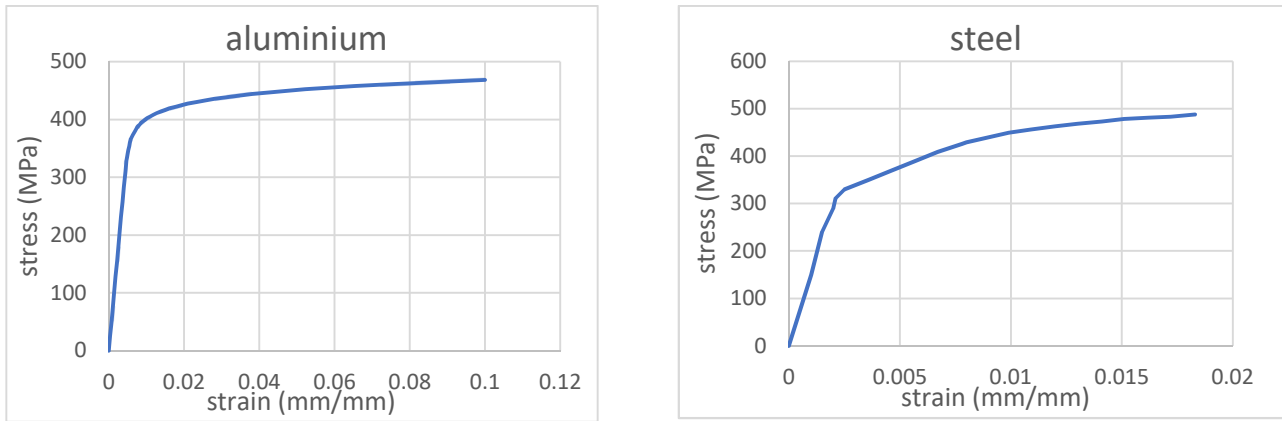


Fig. 3. True stress-strain curve for steel and aluminium alloy (material C and D)



Fig. 4. Buckling test of the unstiffened shell with cutout

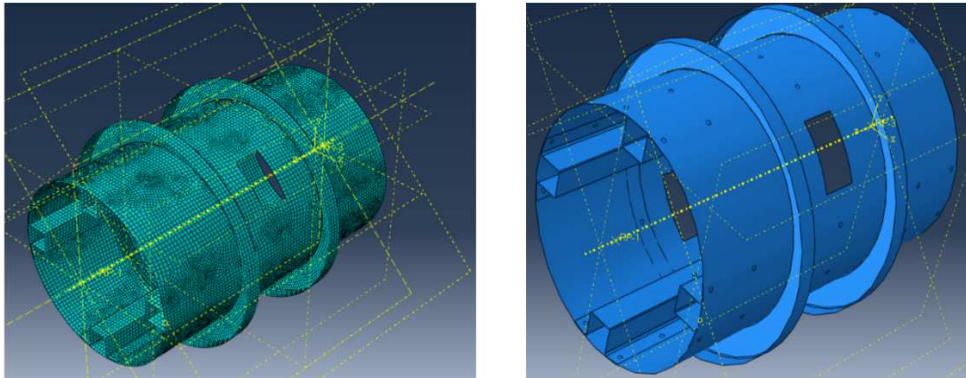


Fig. 5. Typical FE model of the stiffened cylindrical shell

2.2. Experimental set up and boundary conditions

The tests were conducted by Zwick Roell tensile/compression testing machine for two types of steel and aluminum shells with and without stiffeners. Two rigid plates supported ends of the shell as it can be seen in Fig 4. The lower plate is fixed. However, a centric displacement of 2 cm was applied to the upper rigid plate, at very low speed (1 mm/min). Therefore, the test was carried out in displacement control mode, and the Zwick machine automatically recorded the changes in applied load and the amount of compression of the shell at any moment.

2.3. FE modelling of test specimens

At first, the stress convergence is investigated in the longitudinal and tangential direction to obtain the proper mesh size. Linear shell elements S4R are used for the shell and stiffeners which are joined by rivet, as shown in Fig 5.

For applying boundary conditions, in order to numerically analyze the buckling similar to what was done exactly in the experiments, a centric displacement equal to 2 cm was applied to the rigid plates. Additionally, three components of translation (U_x, U_y, U_z) of the lower rigid plates are constrained, and all components of translation except in Z-direction are constrained for the other end (upper rigid plate).



Table 2. Mechanical properties of the considered shell materials

Type	Material	Elasticity modulus E (GPa)	Poisson's ratio ν
A	Steel	207	0.29
B	Aluminum 7075	71.7	0.33

3. FE modelling

3.1. Materials and procedures of unstiffened shell

It is expensive and time-consuming to carry out buckling tests in real dimensions and also manufacturing the test specimens with minimum imperfection is difficult. Therefore, it can be worthwhile to analyze numerically. In addition, several researchers found that there was an excellent correlation between the experimental and nonlinear FE analysis, so the numerical analysis is helpful due to making an acceptable assess of structural behavior of shells.

However, numerical analysis should be analyzed carefully because engineering structures have many imperfections which born during fabricating. Thus, the geometrical imperfections must simulate properly. Moreover, the physics of problem must properly be modelled in numerical analysis to achieve reliable results.

Nonlinear analysis in Abaqus software is based on first order shear deformation theory. Accordingly, it is assumed that transverse shear strain is remained constant through the thickness (transverse inextensibility). Another assumption is that the transverse normal do not resist perpendicular to the mid-surface after deformation.

A thin-walled cylindrical shell is analyzed. At first, the stress convergence is investigated in the longitudinal and tangential direction to obtain mesh size properly. Linear and geometric nonlinear buckling analysis of the cylindrical shell is employed respectively. The linear buckling is used for estimating applied force in nonlinear analysis and it is also used for adding geometric imperfection to FEM model to attain realistic results since deriving mode shapes is the best way to simulate geometric imperfection in specimens. Incremental iterative nonlinear solver (static-Riks) has been employed to trace the equilibrium pre- and post-buckling path. It should be noted that both static-Riks and Dynamic-explicit analysis have acceptable accuracy but the run-time of dynamic method is much more longer than the static one. However, each buckling problem is a dynamic one.

Nonlinear analysis of structures in displacement control or load control fail in many cases because they are unable to capture unstable responses, so both of them must be varied in to solve the problem. The Arc Length Method, or also commonly called "the modified Riks method" is a solution method where the path through a converged solution, at any step, traces a direction orthogonal to the tangent of the solution curve. In this method, both the displacement and the load vary. The basic concept of this method is that firstly, a response is predicted by an incremental force. Then enough iterations are necessary for convergence and also to reach the correct solution.

Geometrical dimensions of cylindrical shell are middle radius 625 mm, length 2125 mm and thickness 1mm. The cylindrical shells used for this part are made of steel and aluminum 7075 with the same geometrical shapes. The stress-strain curve of steel and Mechanical properties of the material are presented in Fig 6 and Table 2. Stress-strain behavior of Steel A is a bilinear elastoplastic model. Test data can be provided as tables of yield stress values versus equivalent plastic strain. Von Misses yield criterion, and isotropic hardening rule is used for plastic modelling. As the material yields, the inelastic strain increment is in the direction of the normal to the yield surface. Stress-strain behavior of Material B exhibit power-law model. At least eight points can be defined to estimate the actual behavior of this plastic model.

The specimens have 2 rectangular cutouts in mid-height position symmetrically. Length and width of the rectangular cutout are 270 and 170 mm, respectively. Boundary condition used in this study is as follows, one end of the shell has fixed support (all degrees of freedom in the lower edge of shell are constrained) and the other end (upper edge of shell) is constrained except in the direction of the z axis. In addition, axial concentrated compressive load is applied to center of the upper edge of shell in the Z-direction. Linear shell element S4R, which is a four-node element with six degrees of freedom per node, was used to discretize the cylindrical shell. The meshed specimen is shown in Fig. 7.

3.2. FE modelling of the stiffened shell

In this part, by adding stiffeners to the steel (table 1-material A) shell, the stiffened shell will be analyzed. The shell was reinforced by 2 types of longitudinal (stringer) and circumferential (rib) stiffeners. 8 stringers and 4 ribs are merged inside the cylindrical shell. Linear shell elements S4R are used for the structures. S4R corresponds to First-order shear deformation theory used for modelling shell. Geometrical and mechanical properties of structures are the same as the steel shell, as explained in the previous section (material A). Geometric dimensions of stiffeners are presented in Figs 8 and 9. The thickness of the stiffeners is 1.5 mm. Boundary conditions and loading are the same as the case of the unstiffened shell (section 3.1).

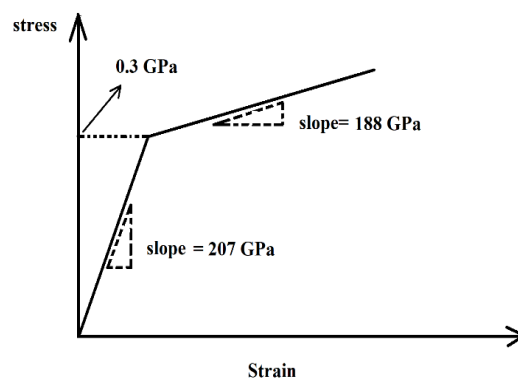


Fig. 6. Stress-plastic strain curve of steel (type A)



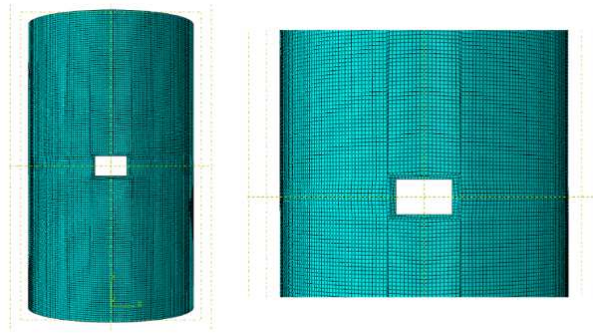


Fig. 7. A sample of FEM mesh

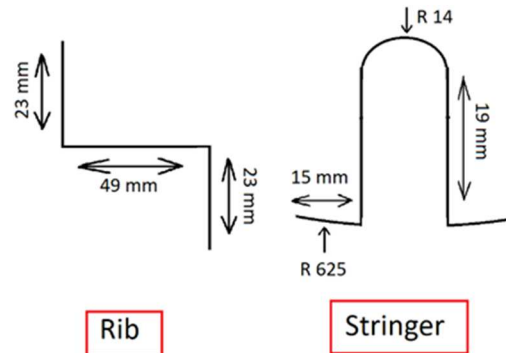


Fig. 8. Cross-sectional dimensions of stiffeners

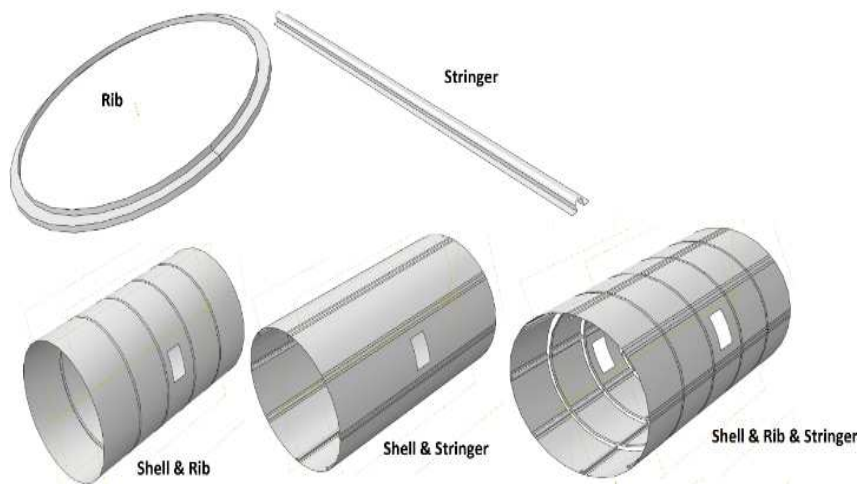


Fig. 9. Perspective of the physical model of stiffened shells with cutout

At first, the stress convergence is investigated in the longitudinal and tangential direction to obtain the proper mesh size. Linear and geometric nonlinear buckling analysis of the cylindrical shell have been accomplished. (Strong form of stiffened cylindrical shell is derived by using Hamilton principle and presented in appendix.)

4. Experimental results

Since test specimens were not ideal, and they had many geometrical imperfections, imperfection coefficient is used for the more accurate evaluation of post-buckling behavior. Imperfection coefficient may be defined as:

$$\xi = \frac{W^*}{t} \quad (1)$$

where W^* is the maximum imperfection amplitude, ξ is imperfection coefficient and t is the thickness of the shell. Superposition of the first four mode shapes with the same imperfection coefficient are used for the simulation in order to the results be closer to the reality. The imperfection coefficients of 0.2, 0.5 and 1 are considered (Table 3). As an illustration, the first four mode shapes of steel stiffened shell is presented in Fig 10. As observed, the deformations of mode shapes are limited around the cutouts edges. Additionally, the protrusions and depressions around the cutout edges change frequently in different mode shapes.



Table 3. Different Imperfection coefficient for numerical modeling

Number of models	Imperfection coefficient
Numerical 1	$\xi = 1$
Numerical 2	$\xi = 0.5$
Numerical 3	$\xi = 0.2$

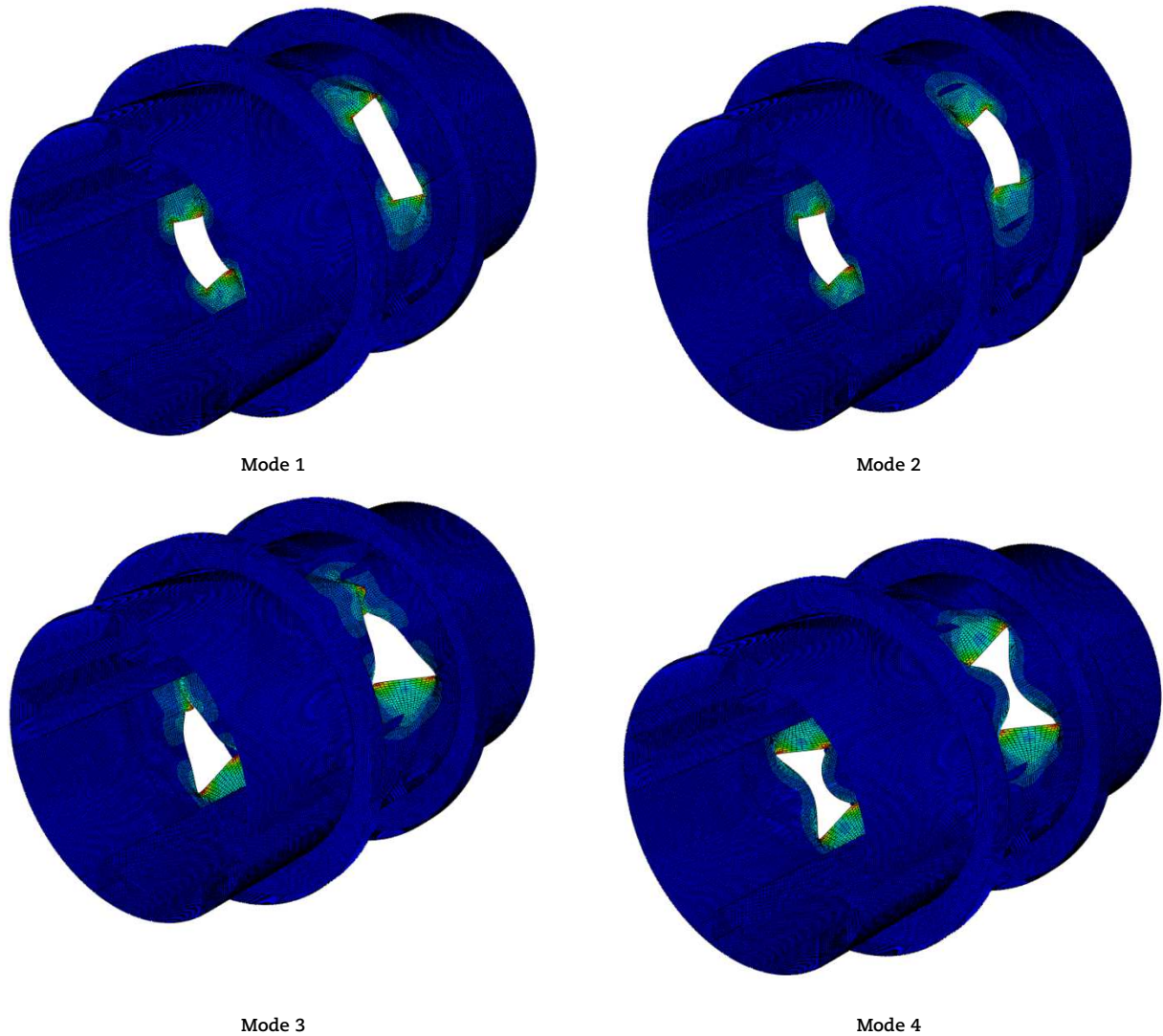


Fig. 10. The first four mode shapes of steel stiffened shell

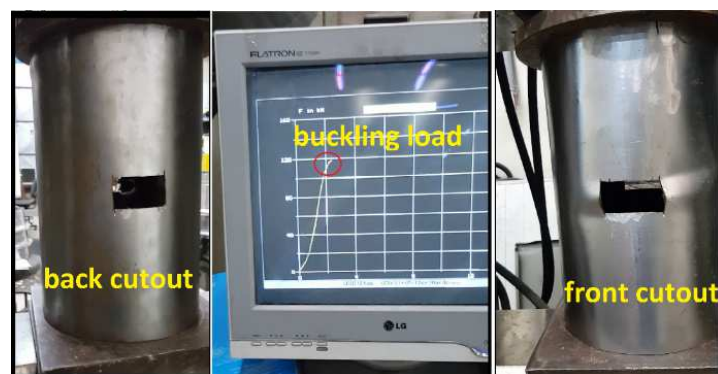


Fig. 11. The instant of local buckling in steel cylindrical shell

4.1. Unstiffened Steel and Aluminium shell (material C and D)

The instant of local buckling of steel shell is shown in Fig 11. The first local buckling of the structure appears in the form of the first mode (only the edges of one of the cutouts are buckled). As the compressive load increases, other mode shapes appear in the structure. As it can be seen in Fig. 12, quite similar buckling deformation is observed in the experiment as well as in the FE modelling.

Fig. 13 shows the experimental force-displacement diagram for the cylinder compared with FE results for different imperfection coefficient values (ξ). The curve designated by numerical 1 corresponds to $\xi = 1$ as stated in Table 3 and is closer to experimental curve than the others. The difference in the experimental and numerical curves in Fig 13 in some displacements may be due to defects in the structure. There was a variety of geometrical imperfections in specimens, e.g., the shape of cutout was irregular rectangle. In addition, another mode shapes may be more similar to the actual defect of the structure than the superposition of the first four mode shapes.

In aluminium shell (material D) specimen, after the cylinder had been buckled, immediately the seam welding of cylinder which was near the cutout was torn. So the post buckling path of the experimental curve is not reliable after the sign showing in Figs. 14 and 15.

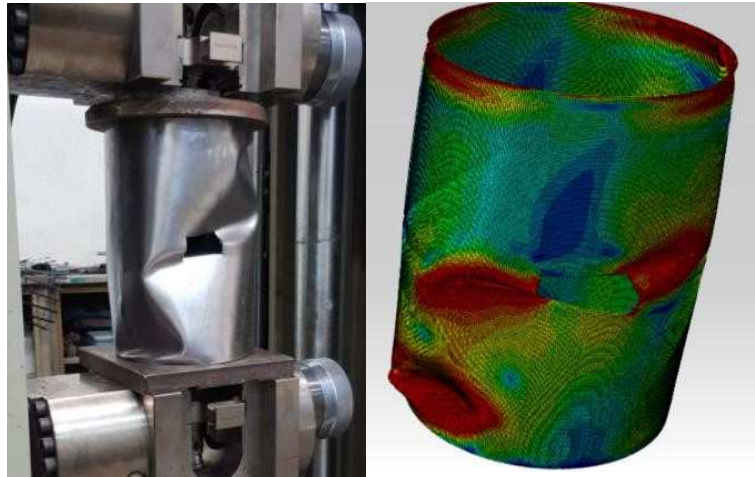


Fig. 12. Comparison of deformations obtained from FE simulation and experimental observations for the shell (front cutout)

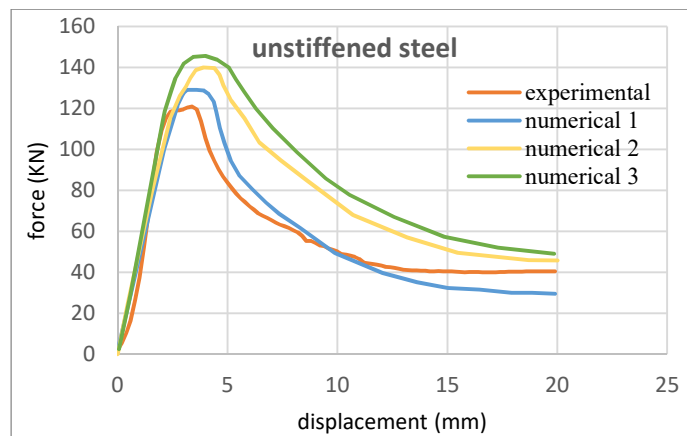


Fig. 13. Comparison of the experimental and numerical force-displacement diagrams for the steel cylinder with cutout

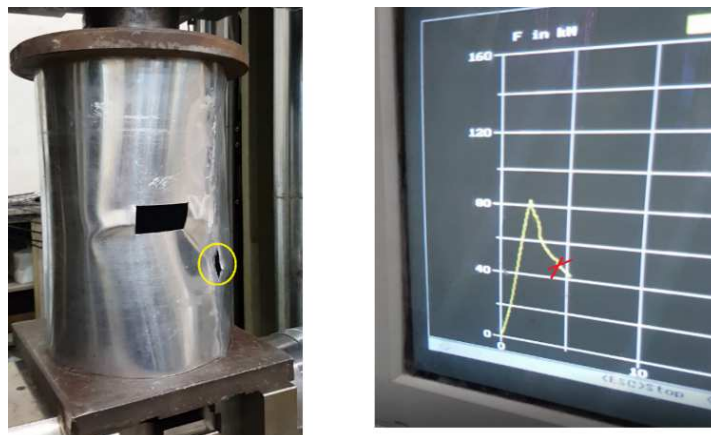


Fig. 14. The moment seam welding tore in aluminum case



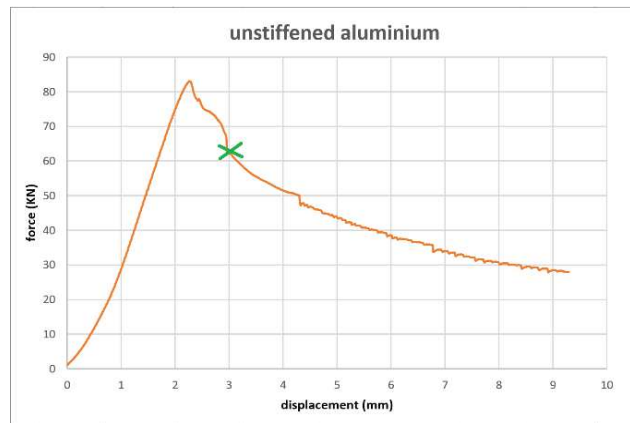


Fig. 15. Load-displacement for unstiffened aluminum specimen at the moment seam welding tore

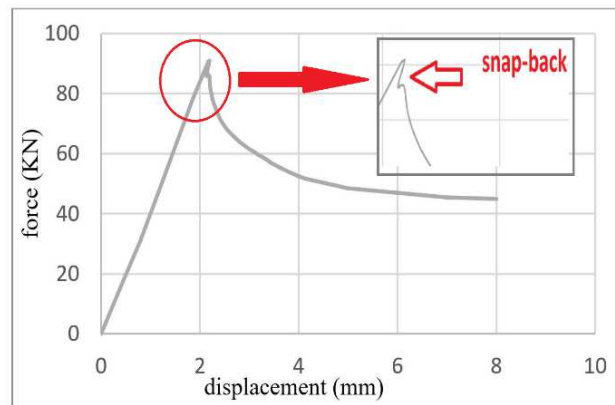


Fig. 16. Load-displacement curve of the upper point of cylindrical aluminum shell (material D)

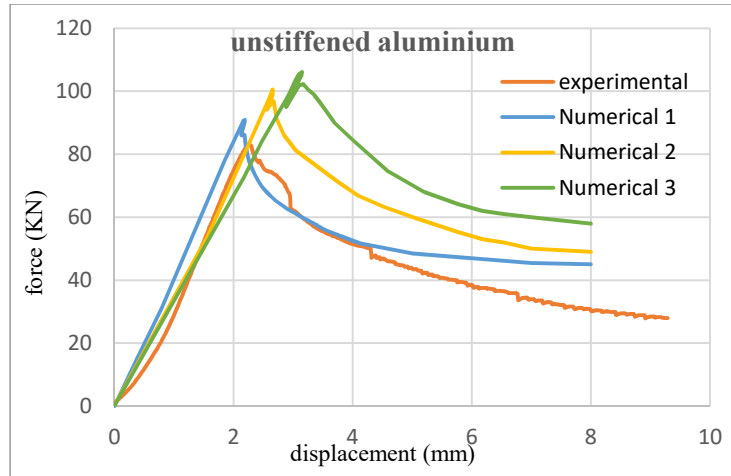


Fig. 17. Comparison of the experimental and numerical force-displacement diagrams for the aluminum cylinder with cutout



Fig. 18. Deformed stiffened steel and aluminum shells

Fig. 16 shows the numerical result for aluminum cylindrical shell, and has an extremely sharp snap-back-turning near the initial post-buckling stage. However, in experimental results, snap-back cannot occur in post-buckling path of the specimen and according to previous explanations, mode transitions lead to this phenomenon. After the snap-back, in this case, the structural analysis cannot endure higher loads. It means the shell fails after this local buckling.

Fig. 17 shows the load-displacement curve obtained from the test, and it is compared with three graphs obtained from the FE analysis (Table 3). As expected, the difference between experimental and numerical curve in Fig 17, where the structure of the welded area has been torn, is large (after 5mm displacement). As the coefficient of imperfection increases, theoretical and experimental data almost converge (before tearing welded zone).

4.2. Stiffened steel and aluminum shell (material C and D)

As shown in Fig 18, at the end of the test, the local deformations are only limited to the midsection of the structure where the cutout is located, unlike the unstiffened steel and aluminum specimens. The other areas of the stiffened cylinders are restrained by stiffeners.

Stiffened steel and aluminium shells are simulated by using material, geometry and assumption of test specimens shown in section 2.1. According to Fig 19, the experimental results of the reinforced cylindrical shells with cutout have been compared with the numerical results for different imperfection coefficients. Increasing imperfection coefficient, numerical and experimental results are going to be close together, as expected.

Fig. 20 shows the experimental force-displacement diagram for the stiffened Aluminium cylinder compared with FE results for different imperfection coefficient values (ξ). The curve designated by numerical 1 corresponds to $\xi = 1$ as stated in Table 3 and is closer to the experimental curve than the others. Nevertheless, the agreement between numerical 1 and experimental curves is not sufficient. For this reason, more mode shapes are added to the previous mode shapes (1 to 4), as geometrical imperfection of the stiffened aluminium shell. The superposition of 8 mode shapes (21 to 24 and 1 to 4) are used in the curve designated by numerical 1**. Imperfection coefficient values of all these 8 mode shapes were selected $\xi=1$.

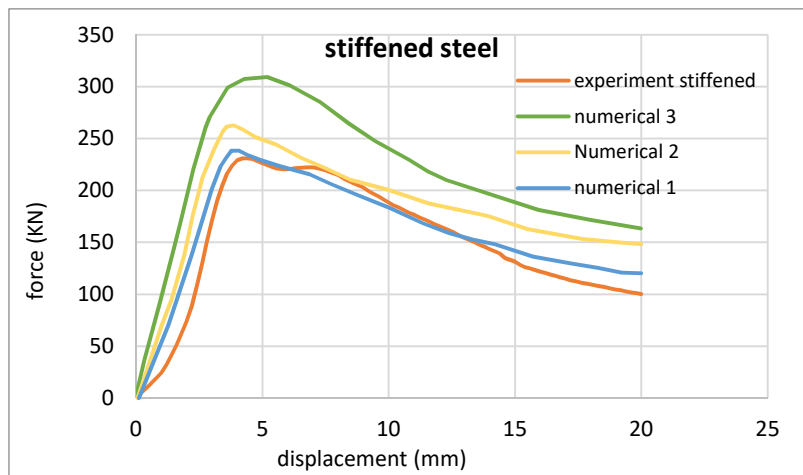


Fig. 19. Comparison of the experimental and numerical force-displacement diagrams for the stiffened steel cylinder with cutout

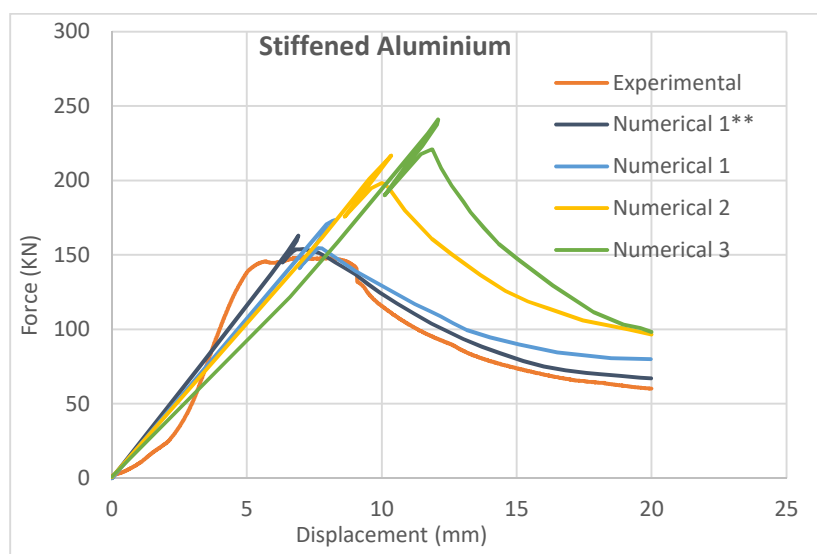


Fig. 20. Comparison of the experimental and numerical force-displacement diagrams for the stiffened aluminium cylinder with cutout



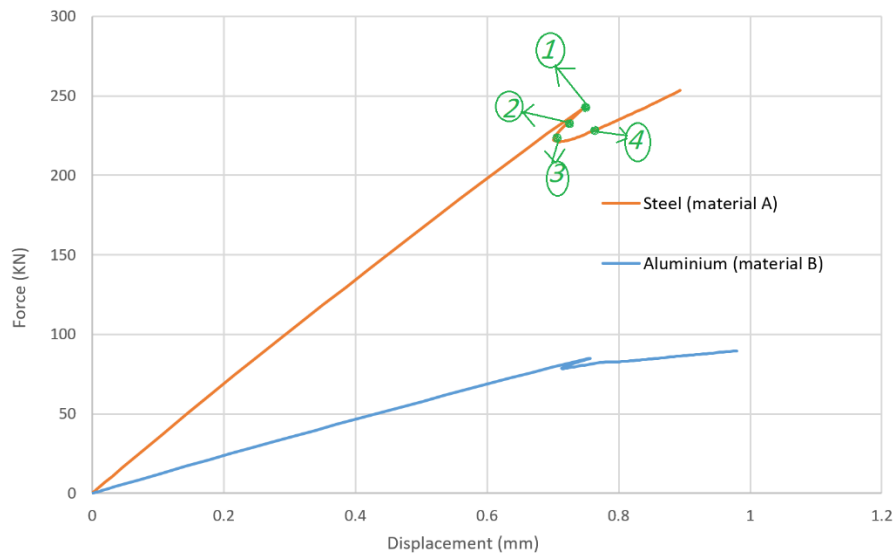


Fig. 21. Load-displacement curve of the upper point of cylindrical steel and aluminium shell

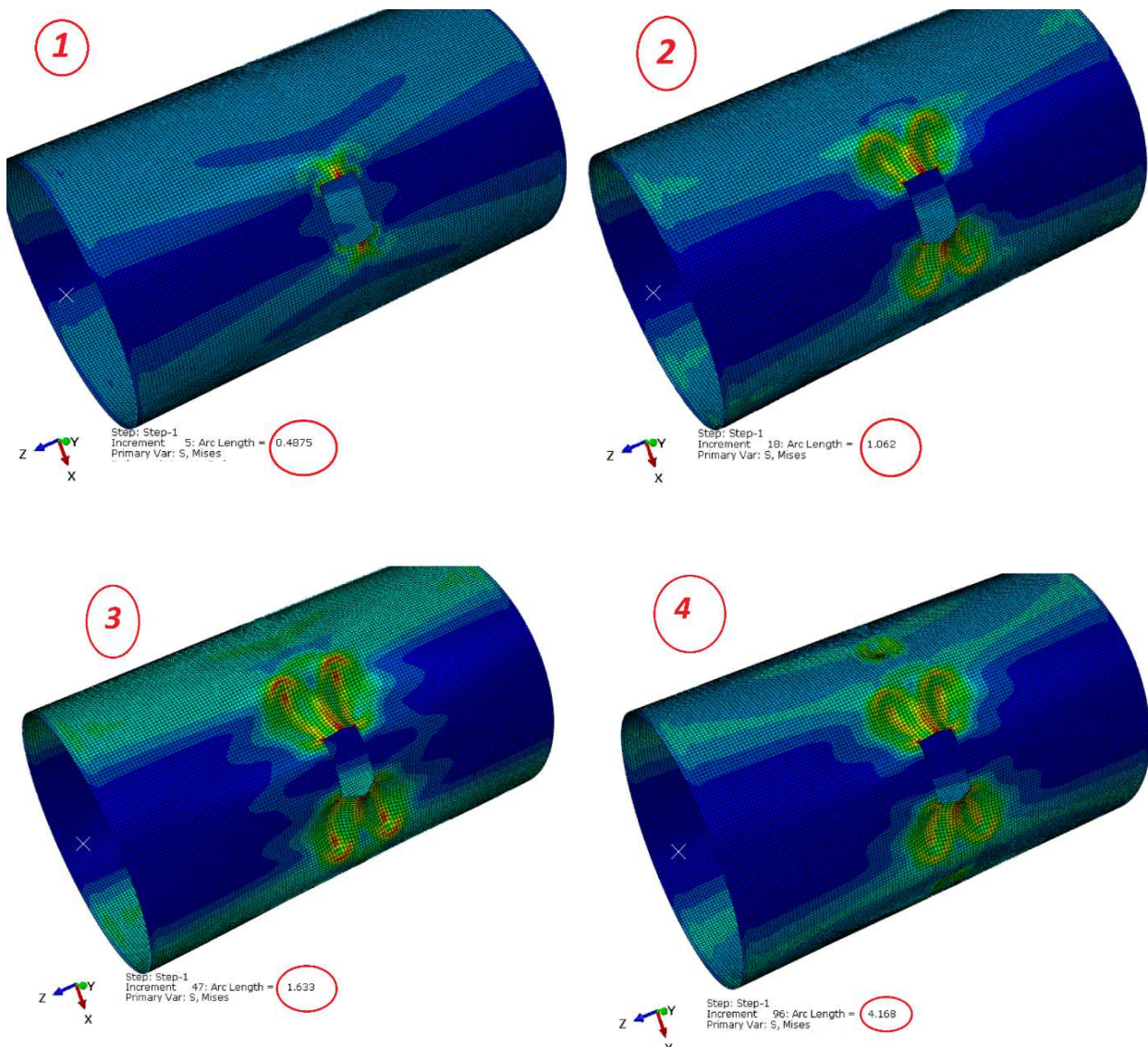


Fig. 22. Different deformation stages of unstiffened steel (material A) derived from nonlinear analysis (Riks solver)



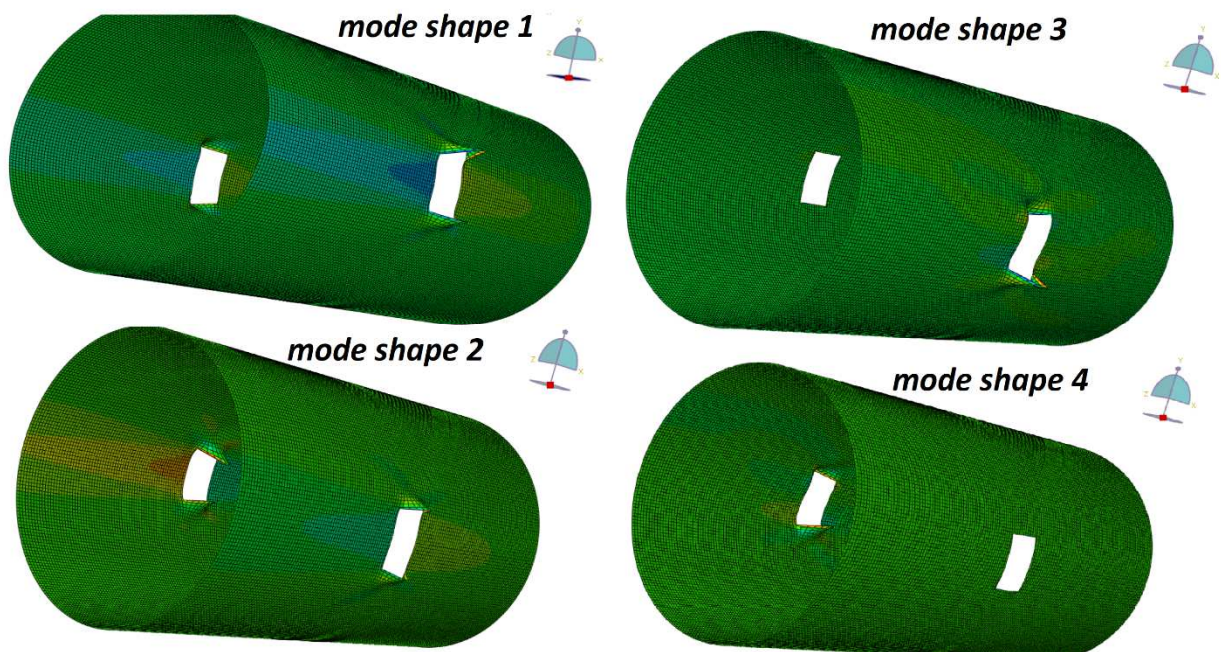


Fig. 23. The first four mode shapes of unstiffened steel (material A)

5. FE results

5.1 Unstiffened Steel and Aluminium shells

The load-displacement curves of the upper point of the steel (table 2-type A) shell are shown in Fig 21 based on the results of FE modelling. According to Liang's (2016) findings, thin-walled cylindrical shells under axial compression often show a snap-back response after buckling. As it can be seen in Fig 21, an extremely sharp snap-back-turning occur near the initial post-buckling phase. For structures which have local buckling in post-buckling behavior, the limited point load before snap-back is considered as the buckling load.

Changing the material of the cylindrical shell to aluminum (Table 2-type B) and repeating the simulation procedure, a snap-back response is again observed and cylindrical aluminum shell has a lower critical load than the steel one in the same values of end shortening.

Buckling and post-buckling stages are considered as unstable behavior. This instability occurs during the buckling process, and mode shapes appear sequentially. This phenomenon is called mode jumps or mode transitions. Therefore, the first mode shape appears at first, and then higher mode shapes are observed, after which higher mode shapes may delete previous mode shapes. It should be mentioned that in this static analysis instead of time, arc length is the progression parameter of static-Riks solver, so in Fig 22, the evolution of buckling modes at 4 different arc lengths derived from nonlinear analysis (Riks solver) are reported, and these 4 points are signed in Fig 21 as well. Considering point 1 in Figs 21 and 22, it is observed that the edges of cut out deform at point 1 where the curve reaches to its critical point. Then at point 2, deformation of the structure increases (Fig 22), and the structure loses its strength (Fig 21). As can be obtained from Fig 21, the structure is in its most deformed stage at point 3. However, as can be seen from Fig 22, after point 3 the deformation of the structure decreases at point 4. Consequently, the force-displacement curve in Fig 21 has a positive slope at point 4. The reason of this phenomenon is, as mentioned above, the protrusions and depressions around the cutout edges change frequently in different mode shapes (derived from linear analysis, Fig 23) thus the ruining effect of the one mode shape is deleted by occurring next mode shapes), which is called mode jumping. Therefore, after a negative slope in post buckling stage where specimen had lost its strength, the slope becomes positive.

5.2. Verification of the results of unstiffened shell modelling

In order to ensure the accuracy of reference, cylindrical unstiffened steel shells with 1 cutout analyzed by Riks method are compared with experimental results of Shariati and Rokhi [16] (all boundary conditions, loading and type of elements of Ref. [16] are completely similar to the simulations in section 3). Elasticity modulus of the steel alloy used in this part is $E = 187.73$ GPa, the value of yield stress is $\sigma_y = 212$ MPa and the value of Poisson's ratio is $\nu = 0.3$. Geometry of the shell is shown in Fig 24. The parameters L , D and t , the length, diameter and thickness of the cylindrical shell is selected as 420 mm, 42mm and 0.78 mm, respectively. Parameter a shows the size of the cutout in longitudinal direction of the cylinder, and parameter b shows the size of the cutout along the circumferential axis of the cylinder. The distance between the center of the cutout and the lower edge of the shell is shown by L_0 .

A comparing among the experimental results of Shariati and Rokhi [16] with the FEA results are presented in Table 4. The dimensionless critical buckling load (N/N_{ref} , $N_{ref} = \pi \times D \times t \times \sigma_y$) of cylindrical shells with different shell lengths and cutout positions are shown in Table 4. The results are shown that having cutouts make shells weaker; in addition, shorter shells are less sensitive to the change in cutouts position. The experimental Shariati and Rokhi [16] and numerical post-buckling path for the specimen with $L = 420$ mm, $L_0 = 294$ mm, $a = 8$ mm, $b = 18.15$ mm are compared and excellent agreement was found as is seen in Fig 25.

As previously mentioned, according to Liang's (2016) findings, numerical analysis of thin-walled cylindrical shells under axial compression "often" (not for all dimensions and materials) show a snap-back response after buckling. Also, comparing Figs. 21 and 25 can demonstrate this subject. As can be seen in Fig 25, for an unstiffened steel cylindrical shell with rectangular cutouts we do not encounter any local buckling in its postbuckling path. However, for another steel shell with different dimensions and Young modulus, Fig. 21, a snap back is appeared in postbuckling curve.



Table 4. Comparison between the results of present study and that of Shariati and Rokhi [16]

Model designation	Dimensionless critical buckling load N/N_{ref}	
	present	Reference Shariati and Rokhi [16]
L: 420 mm , L_0 : 294 mm , a: 8 mm , b: 18 mm	0.8825	0.8504
L: 420 mm , L_0 : 378 mm , a: 8 mm , b: 18 mm	0.9306	0.8948
L: 420 mm , L_0 : 210 mm , without cutout	1.0271	1.0549
L: 273 mm , L_0 : 136.5 mm , a: 8 mm , b: 17.6 mm	0.8037	0.8224
L: 120 mm , L_0 : 60 mm , a: 8 mm , b: 17.6 mm	0.9602	0.9392
L: 120 mm , L_0 : 84 mm , a: 8 mm , b: 17.6 mm	0.9777	0.9483

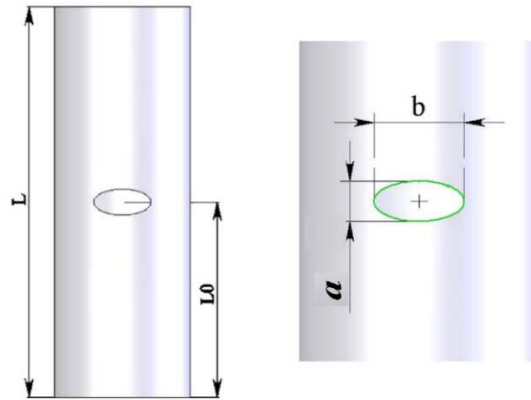
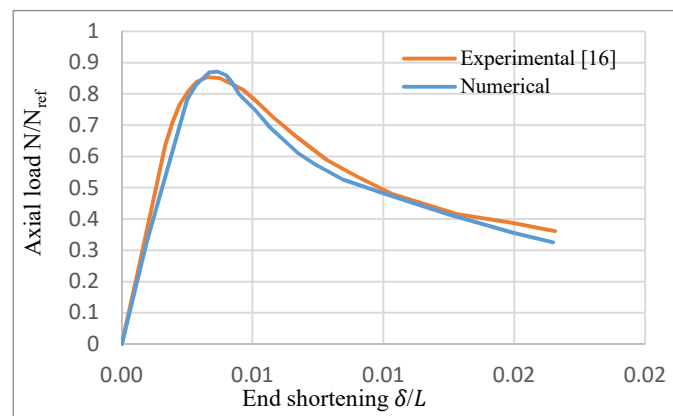
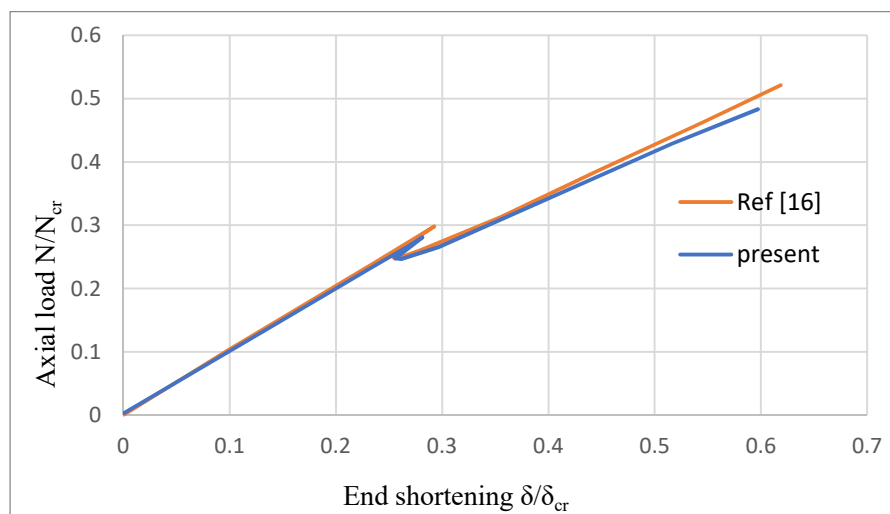

Fig. 24. Geometry of cylindrical shell with Elliptical cutout

Fig. 25. Comparison of the experimental and numerical results for the specimen (L: 420 mm, L_0 : 294 mm , a: 5 mm , b: 18.15 mm)

Fig. 26. Load-end shortening behavior of cylindrical shells of Ref [13] and present results


Table 5. Linear and nonlinear buckling load of unstiffened and stiffened shell

	Linear buckling load (Eigen value) (KN)	Non-Linear buckling load (Riks) (KN)
Unstiffened shell	78.264	242.639
Shell with rib	101.657	268.383
Shell with stringer	154.723	820.021
Shell with rib & stringer	172.573	853.997

The second validation:

A cylindrical unstiffened aluminium shell with a cutout is now analyzed by Riks method the results are compared to the experimental results of Ref. [13]. In this reference, Elasticity modulus of the 6061-T6 aluminium alloy used is $E = 68.948$ GPa and the value of Poisson's ratio is $\nu = 0.33$. The parameters L , D and t , the length, diameter and thickness of the cylindrical shell is selected as 200 mm, 40mm and 0.0889 mm, respectively. The shell has one square cutout $5.3\text{mm} \times 5.3\text{mm}$ and corner chamfer of 0.25mm, the cutout is at the center of the shell. The dimensionless critical buckling load (N/N_{ref} , $N_{ref} = E/\sqrt{3(1-\nu^2)} \times t^2/R$, $N_{cr} = 16.6639$ N/mm) is presented in Fig 26 as a function of dimensionless end shortening (δ/δ_{cr} , $\delta_{cr} = (N_{cr} \cdot L)/E \cdot t$) of the cylindrical shell.

Superposition of the first three mode shapes with the same imperfection coefficient are used for the simulation in order for the results be closer to the reality. An imperfection coefficient of 0.05 is considered. For applying boundary conditions, three components of translation (U_x, U_y, U_z) of the lower edge are constrained, and all components of translation except in Z-direction are constrained for the other end (upper edge). Additionally, a uniform pressure loading is applied at the top edge of the shell.

It is seen from Fig 26 that a very good agreement exists between the results. Owing to the stress concentrations caused by cutouts, regions near the corner of cutouts yield soon after the critical load is reached. Thus, at first local deformations of the shell occur near the cutouts then load decreases due to mode changes and appearing higher mode shapes which is called "buckling capacity hardening" phenomenon [13], then the load increases again. On the other hand, as the local buckled areas appear they will connect to each other leading to global buckling.

5.3. Stiffened shell (material A)

Eigen-value and Static-Riks solvers were employed to derive linear and nonlinear loads of steel shell with stiffeners. As shown in Table 5, the positive impact of each stiffener in increasing buckling load is presented. In addition, Post buckling analysis of shell with stiffeners are presented in Fig 27. As expected, the effect of load proportion on the buckling load of stringer-stiffened cylindrical shell is stronger than rib-stiffened one. While the post-buckling path shows the strength of rib-stiffened cylindrical shells is stronger than the other one in post-buckling areas. It means by using rib as a stiffener, the shell will tolerate higher loads in post-buckling path. Therefore, in order to strengthen shells in terms of buckling load and post-buckling path, both rib and stringer stiffeners are assembled. The evolution of buckling modes at 4 different arc length derived from nonlinear analysis (Riks solver) are reported in Fig 29, and these 4 points are signed in Fig 27 as well. By comparing point 1 in Figs 27 and 29, it is observed that the edges of cut out deform at point 1 where the curve reaches to its critical point. Then at point 2, deformation of the structure increases (Fig 29), and the structure loses its strength (Fig 27). However, as can be seen from Fig 29, the deformation of the structure decreases at point 4. Consequently, the force-displacement curve in Fig 29 has a positive slope at point 3. Then, the deformation changes again (point 4) while the curve has still positive slope.

As previously mentioned, the first mode shape appears at first, and then higher mode shapes are observed, where higher mode shapes may delete previous mode shapes. Therefore, after a negative slope in post buckling stage where specimen had lost its strength, the slope becomes positive. Deformed shape of the stiffened cylindrical shell is shown in Fig 29. As it can be observed, owing to the stress concentrations the deflections are just limited around cutout edges and between stiffeners.

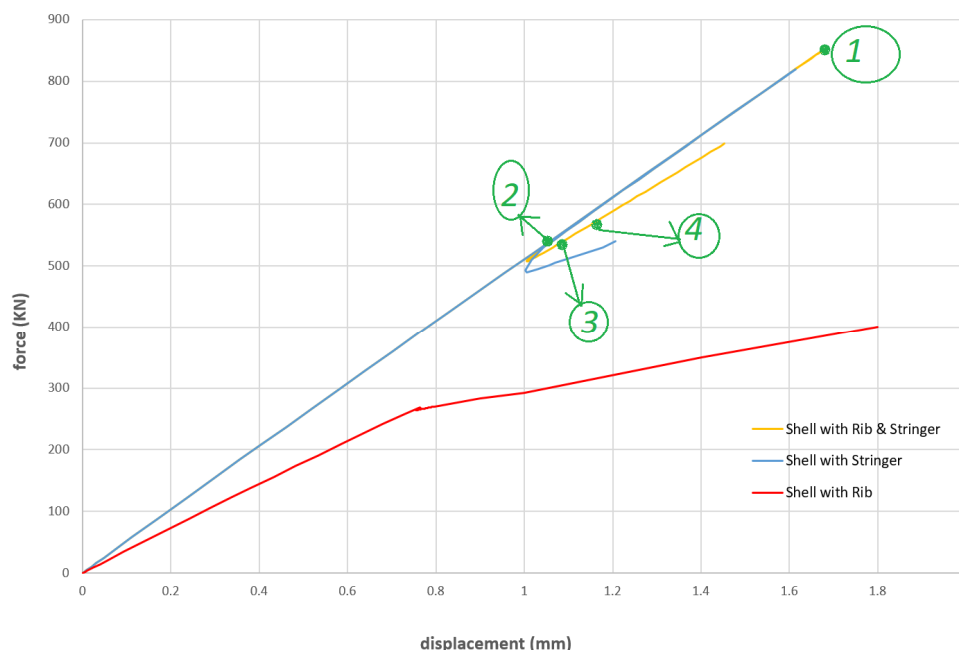


Fig. 27. Load-shortening of stiffened cylindrical shell (material A)-The evolution of first four modes shapes are shown as number 1 to 4



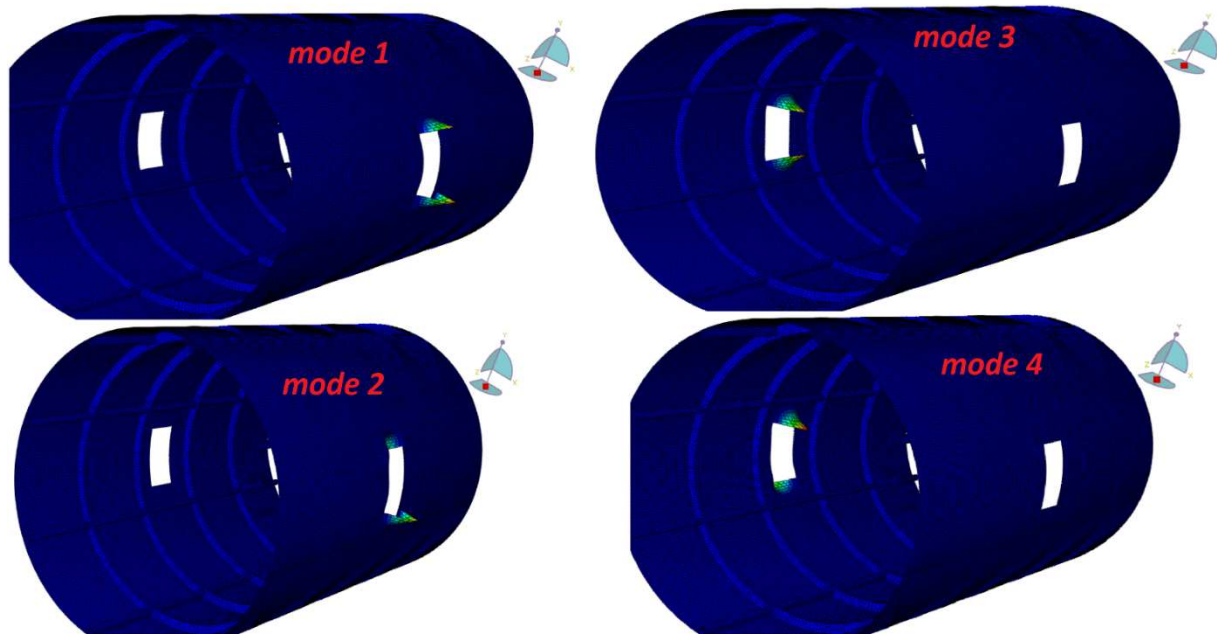


Fig. 28. First four mode shapes of stiffened steel shell

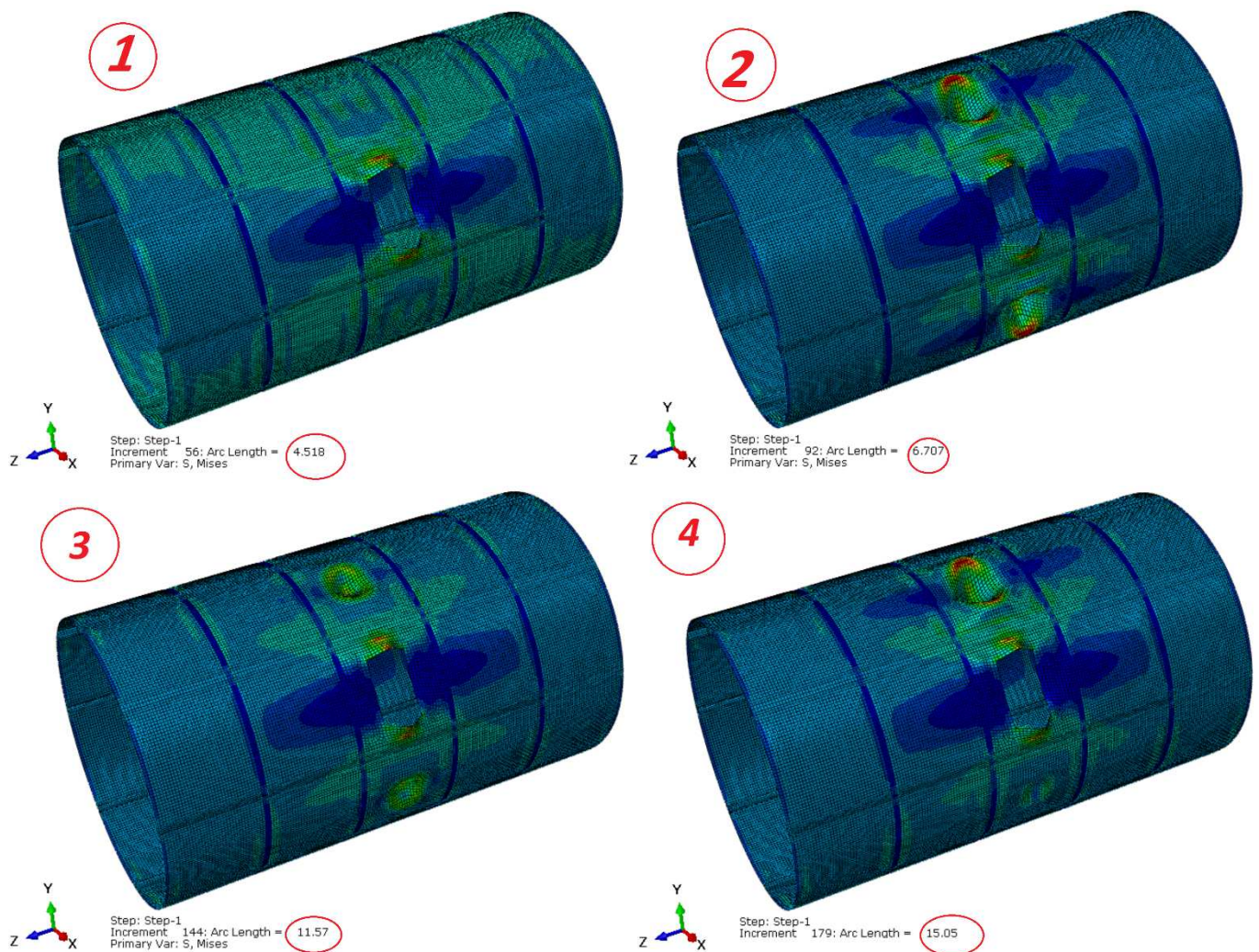
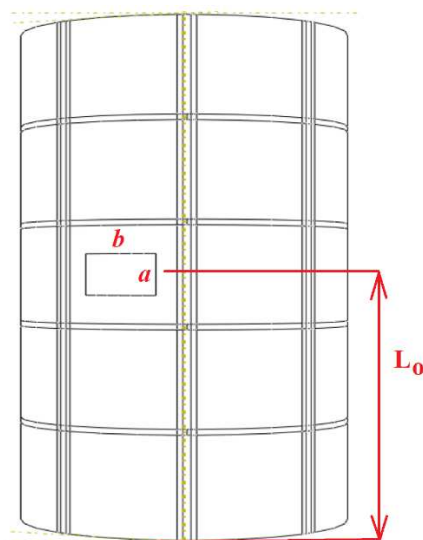
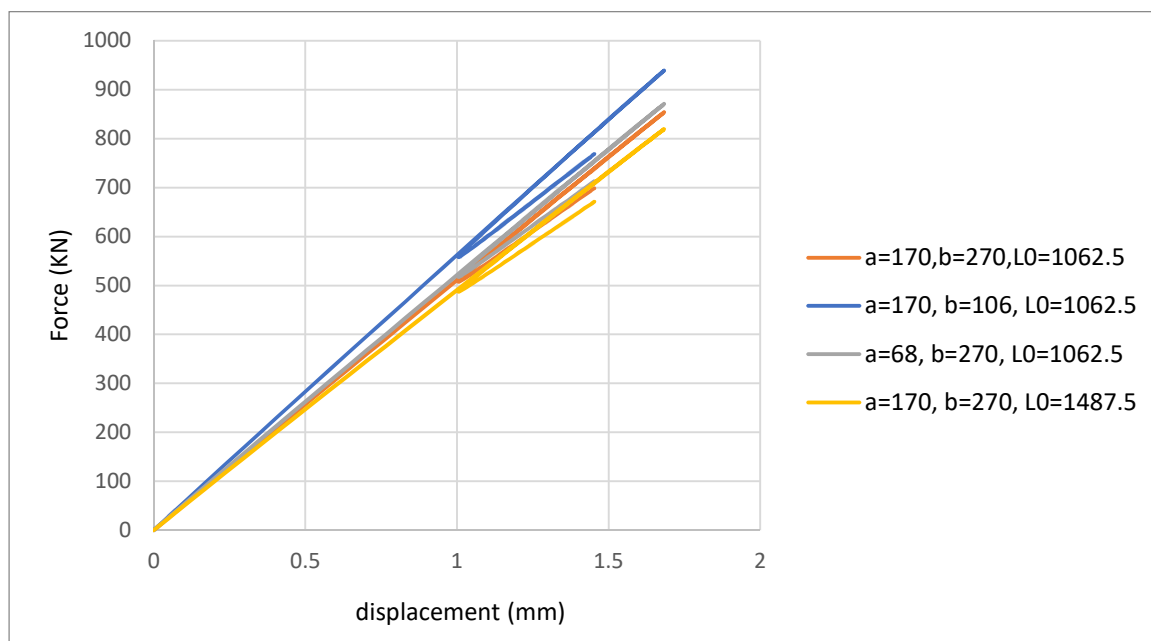


Fig. 29. Local buckling of stiffened cylindrical shell (material A)



Table 6. Buckling loads for different size and location of cutouts

a (mm)	b (mm)	L_0 (mm)	Buckling load (KN)
170	106	1062.5	915.307
170	170	1062.5	889.125
170	270	1062.5	853.997
170	310	1062.5	834.693
68	270	1062.5	875.550
100	270	1062.5	864.045
170	270	1062.5	853.997
210	270	1062.5	846.901
170	270	1487.5	828.005
170	270	637.5	872.633

**Fig. 30.** Geometry of cylindrical shell with rectangular cutout**Fig. 31.** Load-displacement curve of some cases mentioned in Table. 6

Owing to the stress concentrations caused by cutouts, regions near the corner of cutouts yield soon after the critical load is reached. Thus, at first local deformations of the shell occur near the cutouts then load decreases due to mode changes and appearing higher mode shapes, then the load increases again.

On the other hand, as the local buckled areas appear they will connect to each other leading to global buckling. Adding stiffener prevents the connection of these local buckling. The stringers are placed in longitudinal direction that prevent the axial compression and ribs are placed in circumferential direction which prevent the deflections of structure. Thus, the deformations are limited between stiffeners and near cutout edges (compare Figs. 21 and 27 that are unstiffened and stiffened steel shells, respectively).

5.4. The effect of size and location of cutouts on the buckling loads

Geometrical parameters of cylindrical shell are shown in Fig 30, where L_0 , a , b are the distance between the center of the cutout and the lower edge of the shell, the size of the cutout in longitudinal direction of the cylinder, and the size of the cutout along the circumferential axis of the cylinder, respectively.

The effects of size and location of cutouts on the buckling loads are presented in Table 4. As can be observed, when b varied from 106 to 310 mm, while a and L_0 are keeping constant, the buckling load decreases. Besides, when a varied from 76 to 210 mm, while b and L_0 are keeping constant, the buckling load decreases. Although, the buckling load is decreased by increasing both of longitudinal and circumferential dimensions of cutouts, the buckling load is more sensitive to circumferential dimension changes than longitudinal. In addition, when cutouts are closer to the fixed edge (lower edge), the shell become stronger than those at the center.

The load-displacement curve of some cases mentioned in Table. 6 are depicted in Fig. 31. The first dimension set considered is: $a=170$ mm, $b=270$ mm and $L_0=1062.5$ mm. Then we compared the postbuckling curves of other cases with this one. By keeping all dimensions constant and changing just one dimension it can be seen that; If a decreases by 60% ($a=68$ mm), the buckling load will increase by 7%. For other case, if b decreases by 60% ($b=106$ mm), the buckling load will increase 2%. If the cutouts location changes to $L_0=1487.5$ mm, the buckling load will decrease by 7%.

6. Conclusion

The load region that a structure enters after buckling is post-buckling. Generally, before final failure occurs, there may be considerable load capacity beyond buckling. Also, it can help to understand how a structure is likely to fail when the load gets too high. In shell with cutout, local buckles are mostly near the cutout edges. Although, the buckling load is decreased by increasing both of longitudinal and circumferential dimensions of cutouts, the buckling load is more sensitive to circumferential dimension changes than longitudinal. In addition, when cutouts are closer to the fixed edge (lower edge), the shell become stronger than those at the center. For all cutout shapes, critical buckling load decreases when cutout area is increased. Also, by changing the shape of cutouts and remaining the cutout area constant, it was observed that the buckling load did not change noticeably. However, rounded shapes are less critical. Thus, the cut out area is the most significant parameter on the critical buckling load. The effect of load proportion on the buckling load of the stringer-stiffened cylindrical shell is stronger than the rib-stiffened one. In other words, the buckling load value is remarkably enhanced about 4 times by using stringer as stiffeners. In addition, by using rib as stiffener, the shell will endure higher loads up to 12% in post-buckling path. Therefore, in order to strengthen shells in terms of buckling load and post-buckling path, both rib and stringer stiffeners are assembled. Nonlinear analysis of cylindrical steel and aluminum shells with cutout have shown that often the load-displacement curves of the thin-walled cylindrical shells subjected to axial compression have an extremely sharp snap-back-turning occur near the initial post-buckling stage, and it observed in shells with and without stiffeners. Snap-back, which is a decrease in the amount of both load and displacement indicates this local buckling. Although these local buckling happened, the structure is still endured the higher loads. In these cases, the limited point load before snap-back is considered as the buckling load. Snap-back cannot be seen in experimental results because during the numerical buckling analysis of shells mode shapes appear sequentially, commonly called mode jumps or mode transitions. Therefore, the first mode shape appears at first and then higher mode shapes. In this time, higher mode shapes may delete previous mode shapes.

Author Contributions

A.R. Shahani: planned the scheme, supervision, review and editing. F. Kiarasi: conducted the experiments, simulating with software, validation, writing, review and editing. The manuscript was written through the contribution of all authors. All authors discussed the results, reviewed and approved the final version of the manuscript.

Acknowledgments

Not applicable.

Conflict of Interest

The authors declared no potential conflicts of interest with respect to the research, authorship, and publication of this article.

Funding

The authors received no financial support for the research, authorship, and publication of this article.

Data Availability Statements

The datasets generated and/or analyzed during the current study are available from the corresponding author on reasonable request.

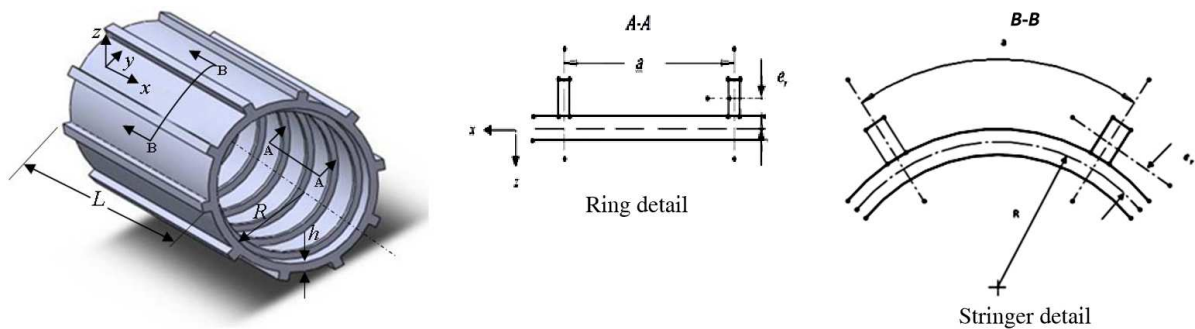
References

- [1] Eslami, M.R., *Buckling and post-buckling of beams, plates, and shells*, Springer, Switzerland, 2018
- [2] Kiarasi, F., Babaei, M., Dimitri, R., Tornabene, F., Hygrothermal modeling of the buckling behavior of sandwich plates with nanocomposite face sheets resting on a Pasternak foundation, *Continuum Mechanics and Thermodynamics*, 2020, 1-22, <https://doi.org/10.1007/s00161-020-00929-6>.



- [3] Van Dyke, P., Stresses about a circular hole in a cylindrical shell, *AIAA Journal*, 3(9), 1965, 1733-1742.
- [4] Tennyson, R.C., The effects of unreinforced circular cutouts on the buckling of circular cylindrical shells under axial compression, *J. Eng. Ind.*, 90(4), 1968, 541-546.
- [5] Brogan, F., Almroth, B.O., Buckling of cylinders with cutouts, *AIAA Journal*, 8(2), 1970, 236-240.
- [6] Almroth, B.O., Brogan, F.A., Marlowe, M.B., Stability analysis of cylinders with circular cutouts, *AIAA Journal*, 11(11), 1973, 1582-1584.
- [7] Toda, S., Buckling of cylinders with cutouts under axial compression, *Experimental Mechanics*, 23(4), 1983, 414-417.
- [8] Hilburger, M., Starnes, J., Waas, A., The response of composite cylindrical shells with cutouts and subjected to internal pressure and axial compression loads, 39th AIAA/ASME/ASCE/AHS/ASC Structures, Structural Dynamics and Materials Conference and Exhibit, 1998.
- [9] Estekanchi, H.E., Vafai, A., On the buckling of cylindrical shells with through cracks under axial load, *Thin-Walled Structures*, 35(4), 1999, 255-274.
- [10] Frulloni, E., Kenny, J.M., Conti, P., Torre, L., Experimental study and finite element analysis of the elastic instability of composite lattice structures for aeronautic applications, *Composite Structures*, 78(4), 2007, 519-528.
- [11] Rahimi, G.H., Poursaeidi, E., Parametric study of plastic strength of cylindrical shells with cutout under bending moment and axial loading, 2004.
- [12] Ghorbanpour Arani, A., Loghman, A., Mosallaei Barzoki, A.A., Kolahchi, R., Elastic buckling analysis of ring and stringer-stiffened cylindrical shells under general pressure and axial compression via the Ritz method, *Journal of Solid Mechanics*, 2(4), 2010, 332-347.
- [13] Han, H., Cheng, J., Taheri, F., Pegg, N., Numerical and experimental investigations of the response of aluminum cylinders with a cutout subject to axial compression, *Thin-Walled Structures*, 44(2), 2006, 254-270.
- [14] Buermann, P., Rolfes, R., Tebmer, J., Schagerl, M., A semi-analytical model for local post-buckling analysis of stringer-and frame-stiffened cylindrical panels, *Thin-Walled Structures*, 44(1), 2006, 102-114.
- [15] Shariati, M., Mahdizadeh Rokhi, M., Buckling of steel cylindrical shells with an elliptical cutout, *International Journal of Steel Structures*, 10(2), 2010, 193-205.
- [16] Shariati, M., Mahdizadeh Rokhi, M., Numerical and experimental investigations on buckling of steel cylindrical shells with elliptical cutout subject to axial compression, *Thin-Walled Structures*, 46(11), 2008, 1251-1261.
- [17] Shariati, M., Mahdizadeh Rokhi, M., Investigation of buckling of Steel cylindrical shells with elliptical cutout under bending moment, *International Review of Mechanical Engineering*, 3, 2009, 1-7.
- [18] Bisagni, C., Cordisco, P., Post-buckling and collapse experiments of stiffened composite cylindrical shells subjected to axial loading and torque, *Composite Structures*, 73(2), 2006, 138-149.
- [19] Yazdani, M., Rahimi, G.H., The effects of helical ribs' number and grid types on the buckling of thin-walled GFRP-stiffened shells under axial loading, *Journal of Reinforced Plastics and Composites*, 29(17), 2010, 2568-2575.
- [20] Shahani, A.R., Mohammadjani, R., Evaluation of FEM instability loads of stiffened cylindrical shells and comparison them with analytical results, *Modares Mechanical Engineering*, 15(6), 2015, 58-68.
- [21] Cheng Z., Niu, J., Zhang, Q., Zhao, C., Xie, J., Buckling behavior of a thin-walled cylinder shell with the cutout imperfections, *Mechanics of Advanced Materials and Structures*, 26(18), 2019, 1536-1542.
- [22] Jiao, P., Chen, Z., Xu, T., Tang, X., Su, W., Effects of ringed stiffener on the buckling behavior of cylindrical shells with cutout under axial compression: Experimental and numerical investigation, *Thin-Walled Structures*, 123, 2018, 232-243.
- [23] Brunesi, E., Nascimbene, R., Effects of structural openings on the buckling strength of cylindrical shells, *Advances in Structural Engineering*, 21(16), 2018, 2466-2482.
- [24] Liang, K., Ruess, M., Nonlinear buckling analysis of the conical and cylindrical shells using the SGL strain based reduced order model and the PHC method, *Aerospace Science and Technology*, 55, 2016, 103-110.
- [25] Vu-Bac, N., Duong, T.X., Lahmer, T., Zhuang, X., Sauer, R.A., Park, H.S., Rabczuk, T.A., NURBS-based inverse analysis for reconstruction of nonlinear deformations of thin shell structures, *Computer Methods in Applied Mechanics and Engineering*, 331, 2018, 427-455.
- [26] Testing, American Society for, Materials, Subcommittee A01, 13 Mechanical, Chemical Testing, Processing Methods of Steel Products, and Processes, Standard test methods and definitions for mechanical testing of steel products: *ASTM International*, 2003.

Appendix



By considering first order shear deformation theory and strain-displacement relations, the equations of strain energy of shell, stringers and ribs are introduced as:

$$U_{\text{Shell}} = \frac{Eh}{2(1-\nu^2)} \int_0^L \int_0^{2\pi} \left[\left(\frac{\partial u}{\partial x} \right)^2 + \frac{1}{R^2} \left(\frac{\partial v}{\partial \theta} - w \right)^2 + \frac{2\nu}{R} \left(\frac{\partial v}{\partial x} \right) \left(\frac{\partial v}{\partial \theta} - w \right) + \frac{1-\nu}{2} \left(\frac{\partial v}{\partial x} + \frac{1}{R} \frac{\partial u}{\partial \theta} \right)^2 \right] R d\theta dx$$

$$+ \frac{Eh^3}{24(1-\nu^2)} \int_0^L \int_0^{2\pi} \left[\left(\frac{\partial^2 w}{\partial x^2} \right)^2 + \frac{1}{R^4} \left(\frac{\partial^2 w}{\partial \theta^2} + w \right)^2 + \frac{2\nu}{R} \left(\frac{\partial^2 w}{\partial x^2} \right) \left(\frac{\partial^2 w}{\partial \theta^2} + w \right) + \frac{2(1-\nu)}{R^2} \left(\frac{\partial^2 w}{\partial x \partial \theta} + \frac{3}{4} \frac{\partial v}{\partial x} - \frac{1}{4R} \frac{\partial u}{\partial \theta} \right)^2 \right] R d\theta dx \quad (A1)$$

$$U_s = \frac{J_s G_s}{2} \int_0^L \left[\frac{1}{R} \frac{\partial^2 w}{\partial \theta \partial x} \right]_{\theta=\theta_s}^2 dx + \frac{E_s}{2} \int_0^L \left[A_s \left[\frac{\partial u}{\partial x} + e_s \frac{\partial^2 w}{\partial x^2} - c_s \frac{\partial^2 v}{\partial x^2} \right]^2 + I_{zs} \left[\frac{\partial^2 v}{\partial x^2} + e_s \frac{1}{R} \frac{\partial^3 w}{\partial x^2 \partial \theta} \right]^2 + I_{yz} \left[\frac{\partial^2 w}{\partial x^2} + c_s \frac{1}{R} \frac{\partial^3 w}{\partial x^2 \partial \theta} \right]^2 \right. \\ \left. + 2I_{yzs} \left[\frac{\partial^2 v}{\partial x^2} + e_s \frac{1}{R} \frac{\partial^3 w}{\partial x^2 \partial \theta} \right] \times \left[\frac{\partial^2 w}{\partial x^2} + c_s \frac{1}{R} \frac{\partial^3 w}{\partial x^2 \partial \theta} \right] \right] dx \quad (A2)$$



$$U_k = \frac{1}{(R+e_k)^3} \left[\frac{E_k I_{zk}}{2} \int_0^{2\pi} \left(w_k + \frac{\partial^2 w_k}{\partial \theta^2} \right)^2 d\theta + \frac{E_k I_{zk} R^2}{2} \int_0^{2\pi} \left\{ \left(\frac{\partial w_k}{\partial \theta} + \frac{1}{R} \frac{\partial^2 u_k}{\partial \theta^2} \right) + \frac{e_k}{R} \left(w_k + \frac{\partial^3 w_k}{\partial x \partial \theta^2} \right) \right\}^2 d\theta \right. \\ \left. + \frac{E_k A_k (R+e)^2}{2} \int_0^{2\pi} \left\{ \left(\frac{\partial v_k}{\partial \theta} - w \right) + \frac{e_k}{R} \left(\frac{\partial v_k}{\partial \theta} + \frac{\partial^2 w_k}{\partial \theta^2} \right) \right\}^2 d\theta + \frac{G_k J_k R^2}{2} \int_0^{2\pi} \left(\frac{1}{R} \frac{\partial u_k}{\partial \theta} - \frac{\partial^2 w_k}{\partial x \partial \theta} \right)^2 d\theta \right] \quad (A3)$$

The total potential energy is written as:

$$V = - \int_0^L \int_0^{2\pi} \frac{q(x)}{2} \left\{ \left[\frac{\partial^2 w}{\partial \theta^2} + w \right] w \right\} d\theta dx - \frac{\beta p}{4} \int_0^L \int_0^{2\pi} \left(\frac{\partial w}{\partial x} \right)^2 R^2 d\theta dx \quad (A4)$$

The Hamilton's principle is expressed as:

$$\Pi = U_{\text{Shell}} + U_{\text{Stringer}} + U_{\text{Ring}} + V_{\text{Loads}} = U_{\text{Shell}} + \sum_{s=1}^M U_s + \sum_{k=1}^N U_k + V_{\text{Loads}} \\ = \frac{Eh}{2(1-\nu^2)} \int_0^L \int_0^{2\pi} \left\{ \left(\frac{\partial u}{\partial x} \right)^2 + \frac{1}{R^2} \left(\frac{\partial v}{\partial \theta} - w \right)^2 + \frac{2\nu}{R} \left(\frac{\partial v}{\partial x} \right) \left(\frac{\partial v}{\partial \theta} - w \right) + \frac{1-\nu}{2} \left(\frac{\partial v}{\partial x} + \frac{1}{R} \frac{\partial u}{\partial \theta} \right)^2 \right\} R d\theta dx \\ + \frac{Eh^3}{24(1-\nu^2)} \int_0^L \int_0^{2\pi} \left\{ \left(\frac{\partial^2 w}{\partial x^2} \right)^2 + \frac{1}{R^4} \left(\frac{\partial^2 w}{\partial \theta^2} + w \right)^2 \right. \\ \left. + \frac{2\nu}{R} \left(\frac{\partial^2 w}{\partial x^2} \right) \left(\frac{\partial^2 w}{\partial \theta^2} + w \right) + \frac{2(1-\nu)}{R^2} \left(\frac{\partial^2 w}{\partial x \partial \theta} + \frac{3}{4} \frac{\partial v}{\partial x} - \frac{1}{4R} \frac{\partial u}{\partial \theta} \right)^2 \right\} R d\theta dx \\ + \sum_{s=1}^M \left\{ \frac{J_s G_s}{2} \int_0^L \left(\frac{1}{R} \frac{\partial^2 w}{\partial \theta \partial x} \right)^2 dx + \frac{E_s}{2} \int_0^L A_s \left[\frac{\partial u}{\partial x} + e_s \frac{\partial^2 w}{\partial x^2} - c_s \frac{\partial^2 v}{\partial x^2} \right]^2 \right. \\ \left. + I_{zs} \left[\frac{\partial^2 v}{\partial x^2} + e_s \frac{1}{R} \frac{\partial^3 w}{\partial x^2 \partial \theta} \right]^2 + I_{yz} \left[\frac{\partial^2 w}{\partial x^2} + c_s \frac{1}{R} \frac{\partial^3 w}{\partial x^2 \partial \theta} \right]^2 \right. \\ \left. 2I_{yzs} \left[\frac{\partial^2 v}{\partial x^2} + e_s \frac{1}{R} \frac{\partial^3 w}{\partial x^2 \partial \theta} \right] \times \left[\frac{\partial^2 w}{\partial x^2} + c_s \frac{1}{R} \frac{\partial^3 w}{\partial x^2 \partial \theta} \right] \right\} dx \\ + \sum_{k=1}^N \left\{ \int_0^{2\pi} \left[\frac{E_k I_{zk}}{2} \frac{1}{R+e_k} \left(\frac{\partial w_k^r}{\partial x} + \frac{1}{R+e_k} \frac{\partial^2 u_k^r}{\partial \theta^2} \right)^2 + \frac{E_k I_{zk}}{2} \frac{1}{(R+e_k)^3} \left(w_k^r + \frac{\partial^2 w_k^r}{\partial \theta^2} \right) \right. \right. \\ \left. \left. + \frac{E_k A_k}{2} \frac{1}{R+e_k} \left(\frac{\partial v_k^r}{\partial \theta} - w_k^r \right)^2 + \frac{G_k J_k}{2} \frac{1}{R+e_k} \left(-\frac{\partial^2 w_k^r}{\partial x \partial \theta} + \frac{1}{R+e_k} \frac{\partial u_k^r}{\partial \theta} \right)^2 \right] d\theta \right\} \\ - \int_0^L \int_0^{2\pi} \frac{q(x)}{2} \left\{ \left[\frac{\partial^2 w}{\partial \theta^2} + w \right] w \right\} d\theta dx - \frac{\beta p}{4} \int_0^L \int_0^{2\pi} \left(\frac{\partial w}{\partial x} \right)^2 R^2 d\theta dx \quad (A5)$$

By replacing u , v and w as below, which are one term of the doubled Fourier series:

$$u = u(x, \theta) = u(x) \sin n\theta \\ v = v(x, \theta) = v(x) \cos n\theta \\ w = w(x, \theta) = w(x) \sin n\theta \quad (A6)$$

in which n indicates the number of circumferential waves.

$$\bar{w} = \frac{w}{R}, \bar{u} = \frac{u}{h}, \bar{v} = \frac{v}{h}, \bar{x} = \frac{x}{L} \\ \bar{J}_k = \frac{J_k}{Rh^3}, \bar{e}_s = \frac{e_s}{h}, \bar{c}_s = \frac{c_s}{h}, \bar{E}_s = \frac{E_s}{E}, \bar{I}_{zs} = \frac{I_{zs}}{Rh^3} \\ \bar{E}_k = \frac{E_k}{E}, \bar{e}_k = \frac{e_k}{h}, \bar{I}_{zk} = \frac{I_{zk}}{Rh^3}, \bar{I}_{xk} = \frac{I_{xk}}{Rh^3}, \bar{A}_k = \frac{A_k}{h^2} \\ I_{ys} = \frac{I_{ys}}{Rh^3}, \bar{I}_{yzs} = \frac{I_{yzs}}{Rh^3}, \bar{A}_s = \frac{A_s}{h^2}, \bar{J}_s = \frac{J_s}{Rh^3} \\ \alpha = \frac{R}{L}, \zeta = \frac{h}{R}, \psi(\bar{x}) = \frac{q(x)}{pL}, \lambda = \frac{pR(1-\nu^2)}{Eh} \quad (A7)$$

Non-dimensional form of Hamilton's principle is written as:

$$\bar{\Pi} = \frac{2\pi(1-\nu^2)}{\pi RLEh} = \bar{U}_c + \sum_{s=1}^M \bar{U}_s + \sum_{k=1}^N \bar{U}_k + \bar{V} \quad (A8)$$

The non-dimensional strain energy of cylindrical shell:



$$\begin{aligned} \bar{U}_c = & \int_0^1 \left\{ \alpha^2 \xi^2 \left(\frac{d\bar{u}}{d\bar{x}} \right)^2 + (\xi n \bar{v} + \bar{w})^2 - 2\nu \alpha \xi \left(\frac{d\bar{u}}{d\bar{x}} \right) (\xi n \bar{v} + \bar{w}) \right. \\ & \left. + \frac{1-\nu}{2} \xi^2 \left(\alpha \frac{d\bar{v}}{d\bar{x}} + n \bar{u} \right)^2 + \frac{\xi^2}{12} \left[\alpha^4 \left(\frac{d^2 \bar{w}}{d\bar{x}^2} \right)^2 + \bar{w}^2 (1-n^2)^2 + 2\nu \alpha^2 \left(\frac{d^2 \bar{w}}{d\bar{x}^2} \right) \bar{w} (1-n^2) + 2(1-\nu) \alpha^2 \left(n \frac{d\bar{w}}{d\bar{x}} + \frac{3}{4} \xi \frac{d\bar{v}}{d\bar{x}} - \frac{1}{4} \frac{n\xi}{\alpha} \bar{u} \right)^2 \right] \right\} d\bar{x} \end{aligned} \quad (A9)$$

The total non-dimensional strain energy of stringers:

$$\begin{aligned} \sum_{s=1}^M \bar{U}_s = & \sum_{s=1}^M \left\{ \frac{(1-\nu^2)}{\pi} \bar{E}_s [\bar{U}_{s1} + \bar{U}_{s2} + \bar{U}_{s3} + \bar{U}_{s4} + \bar{U}_{s5}] \right\} \\ \bar{U}_{s1} = & \frac{\bar{J}_s \alpha^2 \xi^2 n^2}{2(1+\nu)} \cos^2 n\theta \int_0^1 \left(\frac{d\bar{w}}{d\bar{x}} \right)^2 d\bar{x} \\ \bar{U}_{s2} = & \bar{A}_s \xi \alpha^2 \left\{ \xi^2 \sin^2 n\theta \int_0^1 \left(\frac{d\bar{u}}{d\bar{x}} \right) \left(\frac{d^2 \bar{w}}{d\bar{x}^2} \right) d\bar{x} + \bar{c}_s h^2 \alpha^2 \xi^2 \cos^2 n\theta \int_0^1 \left(\frac{d^2 \bar{v}}{d\bar{x}^2} \right)^2 d\bar{x} - 2 \sin n\theta \cos n\theta \left[\bar{c}_s h^2 \alpha^2 \xi^2 \int_0^1 \left(\frac{d\bar{u}}{d\bar{x}} \right) \left(\frac{d^2 \bar{v}}{d\bar{x}^2} \right) d\bar{x} + \bar{e}_s \bar{c}_s h^2 \alpha^2 \xi \int_0^1 \left(\frac{d^2 \bar{w}}{d\bar{x}^2} \right) \left(\frac{d^2 \bar{v}}{d\bar{x}^2} \right) d\bar{x} \right] \right. \\ & \left. \bar{U}_{s3} = \bar{I}_{zs} h^2 \alpha^2 \xi^2 \cos^2 n\theta \left[\int_0^1 \left(\frac{d^2 \bar{v}}{d\bar{x}^2} \right) d\bar{x} + \bar{e}_s^2 n^2 \int_0^1 \left(\frac{d^2 \bar{w}}{d\bar{x}^2} \right)^2 d\bar{x} + 2 \bar{e}_s n \int_0^1 \left(\frac{d^2 \bar{v}}{d\bar{x}^2} \right) \left(\frac{d^2 \bar{w}}{d\bar{x}^2} \right) d\bar{x} \right] \right. \\ & \bar{U}_{s4} = \bar{I}_{ys} h^2 \alpha^2 [\sin n\theta + \bar{c}_s n \xi \cos n\theta]^2 \int_0^1 \left(\frac{d^2 \bar{w}}{d\bar{x}^2} \right)^2 d\bar{x} \\ & \left. \bar{U}_{s5} = 2 \bar{I}_{yzs} h^2 \alpha^2 \xi \cos n\theta (\sin n\theta + \bar{c}_s n \xi \cos n\theta) \left[\int_0^1 \left(\frac{d^2 \bar{v}}{d\bar{x}^2} \right) \left(\frac{d^2 \bar{w}}{d\bar{x}^2} \right) d\bar{x} + \bar{e}_s n \int_0^1 \left(\frac{d^2 \bar{w}}{d\bar{x}^2} \right)^2 d\bar{x} \right] \right\} \end{aligned} \quad (A10)$$

The total non-dimensional strain energy of Ribs:

$$\sum_{k=1}^N \bar{U}_k = \frac{1-\nu^2}{(1+\xi \bar{e}_k)^3} \bar{E}_k \alpha \xi^2 [\bar{U}_{k1} + \bar{U}_{k2} + \bar{U}_{k3} + \bar{U}_{k4}] \quad (A11)$$

in which:


$$\begin{aligned} \bar{U}_{k1} = & \bar{I}_{zk} \left[\alpha (1 + \xi \bar{e}_k - n^2 \xi \bar{e}_k) \frac{d\bar{w}_k}{d\bar{x}} - \xi n^2 \bar{u}_k \right]^2 \\ \bar{U}_{k2} = & \bar{I}_{xk} [(1-n^2) \bar{w}_k]^2 \\ \bar{U}_{k3} = & \bar{A}_k \frac{(1+\xi \bar{e}_k)^2}{\xi} [\xi n (1+\xi \bar{e}_k) \bar{w}_k]^2 \\ \bar{U}_{k4} = & \frac{\bar{J}_k}{2(1+\nu_k)} \left[-\xi n \bar{u}_k + \alpha n \frac{d\bar{w}_k}{d\bar{x}} \right]^2 \end{aligned}$$

The total potential energy of cylindrical shell under lateral and axial pressure:

$$\bar{V} = \bar{V}_l + \bar{V}_a = -\lambda \int_0^1 \left[\psi(\bar{x}) \bar{w}^2 (1-n^2) + \frac{\beta \alpha^2}{2} \left(\frac{d\bar{w}}{d\bar{x}} \right)^2 \right] d\bar{x} \quad (A12)$$

ORCID iD

Amir Reza Shahani  <https://orcid.org/0000-0002-0070-6260>

Faraz Kiarasi  <https://orcid.org/0000-0003-2171-8188>



© 2021 Shahid Chamran University of Ahvaz, Ahvaz, Iran. This article is an open access article distributed under the terms and conditions of the Creative Commons Attribution-NonCommercial 4.0 International (CC BY-NC 4.0 license) (<http://creativecommons.org/licenses/by-nc/4.0/>).

How to cite this article: Shahani A.R., Kiarasi F. Numerical and Experimental Investigation on Post-buckling Behavior of Stiffened Cylindrical Shells with Cutout subject to Uniform Axial Compression, *J. Appl. Comput. Mech.*, 9(1), 2023, 25–44. <https://doi.org/10.22055/JACM.2021.33649.2261>

Publisher's Note Shahid Chamran University of Ahvaz remains neutral with regard to jurisdictional claims in published maps and institutional affiliations.

